IEEE Access
Multidisciplinary | Rapid Review | Open Access Journal

Received 24 July 2024, accepted 27 August 2024, date of publication 30 August 2024, date of current version 10 September 2024.

Digital Object Identifier 10.1109/ACCESS.2024.3452636

APPLIED RESEARCH

The Non-Metallic Electrical Connector: A New Connector Technology Based on Wireless Power Transfer

JOSHUA S. BENJESTORF[1], (Senior Member, IEEE), VINCENT C. PASCUCCI[1], JULIO V. URBINA[2], (Senior Member, IEEE), AND AKHLESH LAKHTAKIA[3], (Fellow, IEEE)

[1]Non-Metallic Connectors, Inc., Harrisburg, PA 17104, USA
[2]Department of Electrical Engineering, The Pennsylvania State University, University Park, PA 16802, USA
[3]Department of Engineering Science and Mechanics, The Pennsylvania State University, University Park, PA 16802, USA

Corresponding author: Joshua S. Benjestorf (joshua.benjestorf@nmccorporation.com)

This work was supported by Non-Metallic Connectors, Inc. The work of Akhlesh Lakhtakia was supported by robust financial support for his research efforts, from 2006 to 2024.

ABSTRACT Wireless power transfer (WPT) is now ubiquitous, having penetrated almost every industry within the last 20 years, due to certain desirable attributes explained in this paper. Furthermore, WPT is now in an advanced state whereby it is now technically feasible to apply the methods of WPT to the connector industry and surmount commonplace problems that have plagued the electrical connector industry since the invention of the first electrical connector in 1885. Whereas other common technologies have evolved greatly over the last two centuries with the emergence and development of new primary mechanisms, the primary mechanism used in electrical connectors–the electrical contact–has not changed. The electrical contact is the source of many failure modes, several of which can be eliminated by applying the WPT methodology through a new type of connector called the Non-Metallic Connector (NMC). As a result, connectors can now be made entirely contactless, possessing a hermetically sealed interface that is also shockproof. The NMC concept is applicable to both signal transfer and power transfer. NMCs fall into the categories of both near-zone and far-zone technologies, necessitating thereby the introduction of the μWPT in the commonly accepted WPT hierarchy. Appropriate circuit topologies as well as major design challenges are identified for power-transfer NMCs with appropriate methods to overcome those challenges, based on the electrical power handling requirement.

INDEX TERMS Contactless connectivity, electrical contacts, extremely high frequency (EHF), metamaterial, non-metallic connector (NMC), Q-factor, wireless power transfer (WPT).

I. INTRODUCTION

An electrical connector can be defined as an electromechanical system that provides a separable interface between two subsystems of an electronic system without an unacceptable effect on the system performance [1]. One of the first connectors was invented in 1885 by Thomas Tylar Smith and was called the electric-circuit connection. It was a separable interface created to ''enable the electric conductor or conductors. . . to be rapidly and safely brought into connection with the line or main wires'' [2]. The driving force behind its invention was the electrification of homes and buildings that in turn was partly driven by the demand for the newly invented incandescent bulb patented in 1880 by Thomas Edison in the U.S.A. [3] and independently in the U.K. by Joseph Swan [4]. Edison proposed a way to connect electric lamps using the infrastructure that was already in place at the time. His proposal was to use gas pipelines to ground the first terminal on incandescent bulbs [5]. The second terminal connection would have to be wired to the building separately.

A major drawback of Edison's system was that each incandescent bulb needed to be hardwired into the house,

The associate editor coordinating the review of this manuscript and approving it for publication was Diego Masotti.

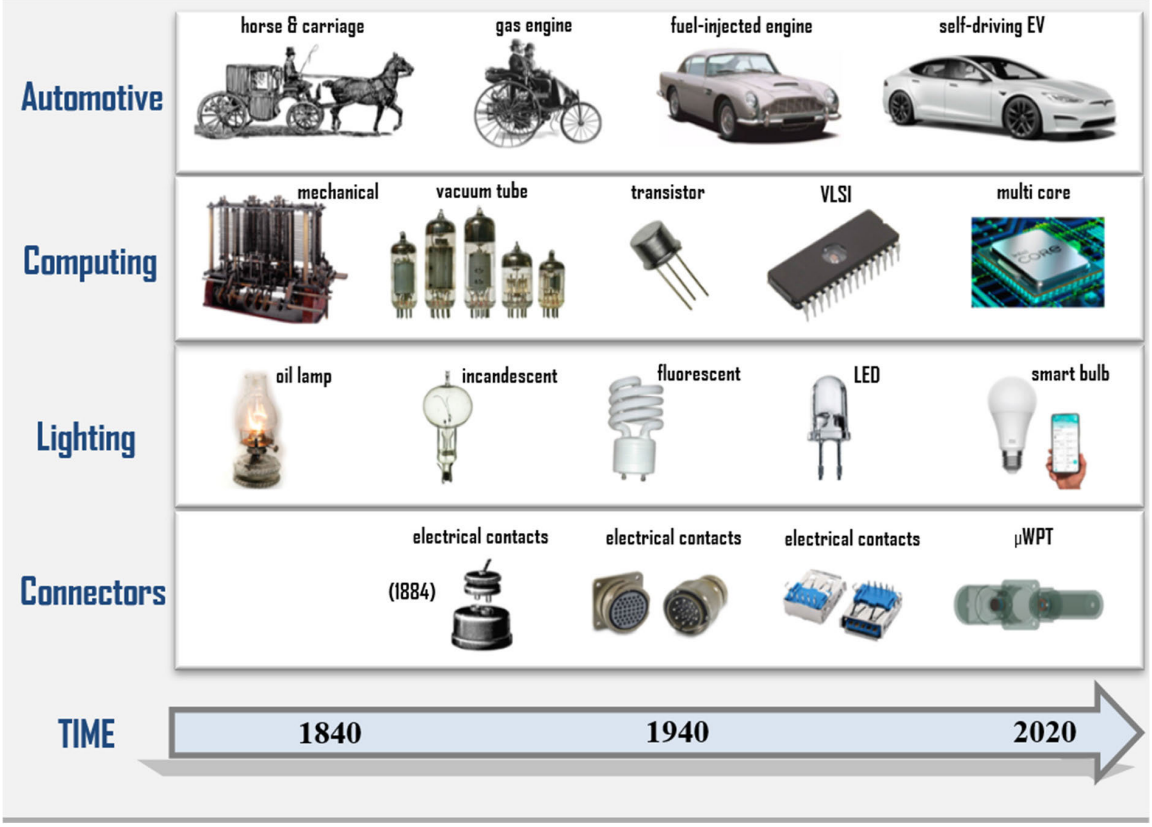

FIGURE 1. Examples of how the primary mechanisms for several industries have changed over time, giving rise to rapid changes within that industry. The connector industry is the only industry that has not undergone any changes to the primary mechanism over this time period until recently.

which made replacements inconvenient. This is where the invention of the first connector concept developed by Smith really showed its value; it was a way to provide a mechanically separable interface between two subsystems of an electrical system. It did not take long after this innovation for other electrical household devices to be introduced such as fans, heating irons, and vacuum cleaners, with all of them to be connected to the electricity mains. The invention by Smith and many other inventions by Harvey Hubbel in the early 20th century introduced different ways to make the contemporary electrical devices of their time compatible with ubiquitous light sockets [6], [7], [8].

When electrical wiring started to be installed in new homes and buildings in the early 20th century, the only method of making connections with wiring was dangerous as it involved: first, twisting a stripped end of each of two wires; second, coating the stripped ends with solder; and third, twisting them together for a firm connection. This method was also very time consuming, and it eventually was eliminated by a new connector design in 1914 by Bill Marr at Eaton Company.

Marr eventually went on to start his own connector company that focused on commercializing his new set-screw connectors from 1926 onwards [9]. That company became the largest manufacturer of the early set-screw connectors for appliances until times changed again and other industries demanded more.

The separable interface made the transportation of radio communications equipment for military aircraft and ships possible during the Second World War, whereas earlier such equipment had to be manually assembled and soldered on site. The invention of solderless termination by AMP, Inc. changed the scenario in 1941 [10], and many other connector companies entered the competition soon after. During the 1940s, a plethora of connectors came on the market for electrical devices of many types, and it was well understood that signal and power connectors had different requirements that would impact electrical performance to determine connector reliability [11], [12], [13]. Therefore, many connector companies in the 1940s and 1950s invested heavily in connector-contact physics, the quality of the electronic connection becoming a major driving force that continued in the decades that followed.

While the specific type of goods or services that an industry offers may never change (e.g., the lighting industry has always been about producing light), the primary mechanisms by which those goods or services are delivered (e.g., better ways of producing light) have changed significantly since the Industrial Revolution began and continue to change. Figure 1 shows several illustrations of the technological evolution over

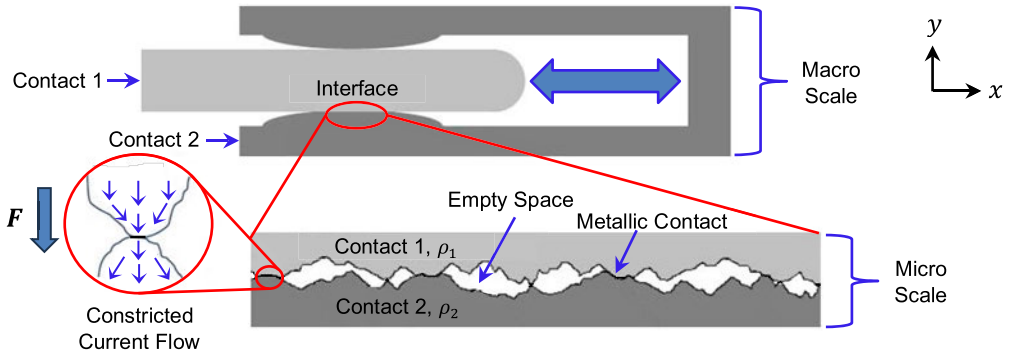

FIGURE 2. Illustration of two electrical contacts making physical contact at the connector interface. On the macroscale, the interface between Contact 1 and Contact 2 appears continuous and smooth, electrical current is restricted to the real contact area on a microscale.

the last two centuries in the automotive, computing, lighting, and connector industries. Over time innovation has given way to better primary mechanisms that have delivered impactful changes for every industry except for one: the connector industry. As a result, the same problems associated with the primary mechanism in standard connectors —- the electrical contact —- continue to this day.

Today, the competition in the connector industry shows no signs of slowing down. Since the turn of the 21st century, the demand for smaller, thinner, and faster consumer-electronics devices continues to rise. Fast urbanization and industrial expansion around the world have given rise to growth within the automotive and telecommunications sectors and the burgeoning adoption of 5G and IoT devices is further propelling the demand for new connectors. The forecasted demand for connectors is expected to grow by a compound annual growth rate of 7.80%, raising the connector-industry value from US $83.5B in 2022 to US $176.13B by 2032 [14]. As the world population and standards of living continue to increase, the demands for energy and different electronic devices will also continue to increase and, consequently, and so will the volume of e-waste [15]. The need for more sustainable engineering practices and cleaner technologies is nowadays more critical than ever.

The rest of this paper is organized as follows. Section II presents the most common failure modes for connectors in terms of electrical-contact physics. Common connector failure modes are exemplified by actual data from connector stress tests to accelerate wear and simulate real-world conditions. Section III introduces a new primary mechanism for connectors using the methods of wireless power transfer (WPT), thereby creating a new connector concept called the non-metallic connector (NMC). This section also identifies the three factors why WPT has remained technically infeasible for connector applications until recently. A historical overview of WPT advancements over the last 150 years shows that WPT technology can now be made both small and efficient enough to make NMCs technically feasible. Section IV introduces NMCs for high-speed signal transfer, establishes how NMCs differ from other WPT systems, introduces micro-WPT (μWPT), and inserts μWPT in the WPT hierarchy [105]. Section V introduces NMCs for power transfer and identifies the relevant circuit topologies that apply to NMCs and engineering basis for it. Three major design constraints limiting NMC power applications are discussed along with potential ways to surmount the constraints. The paper closes with Section VI on the future of NMCs as a new sustainable connector technology that is more energy efficient, less wasteful, and has a lower carbon footprint.

II. PROBLEMS WITH ELECTRICAL CONTACTS

In theory, the creation of a low-resistance separable interface is simple: place two conductive surfaces in contact and apply a sufficient normal force on them. The surfaces must be clean initially and must stay clean to maintain the total area of metal-to-metal contact. Factors which can degrade an existing interface include: (i) reduction of normal force due to stress relaxation and other factors, (ii) electrical contact wear, and (iii) corrosion of various types [16], [17], [18], [19], [20]. The connector industry has done excellent work in managing these problems through the use of specialized plating systems to reduce corrosion and wear, through proper design of contacts to achieve the normal force of appropriate magnitude, and by the judicious use of alloys to manage stress relaxation.

Of the many possible factors that can negatively affect efficiency of electrical contacts, four have been identified as having the most impact. Three of those factors are electrical transition voltage, commutation noise, and erosion resistance. The fourth factor is tribological: physical contact wear that can increase contact resistance via damage to the plating systems in general and fretting corrosion of non-noble plating. These factors can and often do lead to failure, as discussed next.

A. REGIONS OF CONTACT SURFACE AREA, ASPERITIES, AND CONSTRICTION RESISTANCE

In order to create an electrical interface, a region of metal-to-metal contact must be established for electrical current

to freely flow without an unacceptable level of electrical resistance. Figure 2 is an illustration of two electrical contacts at a contact interface. On a macro scale, the contact interface looks continuous and smooth and gives the impression that electrical current can flow freely from Contact 1 to Contact 2 through what is referred to as the *apparent contact region*. This region is made up mostly of empty space and comprises of several other regions, as illustrated in Fig. 3 [21]. When viewed on a micro scale, the contact interface is not planar but has some level of surface roughness. The *real contact region* comprises a quasi-metallic zone containing metal oxides that can allow for some current but not enough to be reliable [22], [23], [24]. The *load-bearing regions* contain oxide films and dust particles, for which they do not provide dependable pathways for the current. The actual electrical interface that allows for good current is made up of many small points of contact, referred to as *asperities* that exist on the highest points of contact between the two contact surfaces. Much smaller relative to the apparent surface and randomly distributed, asperities typically make up less than 1% of the apparent contact region. All asperities contribute together to the total constricted resistance R_C that is conventionally estimated as

$$R_C = \rho\left(\frac{1}{D} + \frac{1}{nd}\right), \tag{1}$$

where $\rho = \rho_1 = \rho_2$ is the resistivity of both Contact 1 and Contact 2 in Fig. 2, D and d are the diameter of the apparent contact region and the average diameter of an individual asperity, respectively, and n is the total number of asperities [22].

From (1) it is clear that electron flow would be less constricted if n were to become very large. Therefore, as the number of asperities increases, the resistance across the contact interface decreases. With sufficient normal force F pressing the two contact surfaces together, the interface resistance R_S between the two contacts is not equal to ρ/D but can be approximated as

$$R_S \approx \rho\sqrt{\frac{H}{F}}, \tag{2}$$

where H is the contact surface hardness [28], [29]. Clearly, increasing F will reduce R_S, and vice versa.

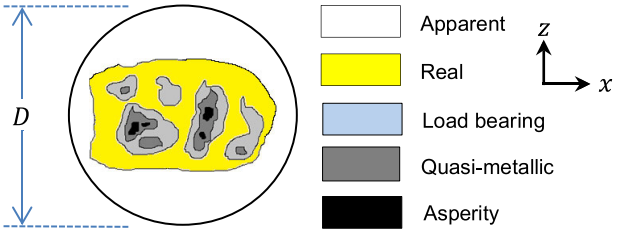

FIGURE 3. A cluster with diameter *D* illustrating the different regions of contact and how current flow is constricted to contact asperities.

A primary intrinsic cause that can influence the reduction of F is stress relaxation which is greatly impacted by temperature.

B. STRESS RELAXATION AND TEMPERATURE

Stress relaxation is a concern in many connector applications and is a potential failure mode of electrical contacts. When two electrical contacts are mated as in Fig. 2, they are deformed resulting in stress that creates the initial normal force F. If the stress in a contact spring formed by two asperities in direct contact were somehow reduced, F would also be reduced causing an increase in R_S as implied by (2). However, while the majority of each asperity's deformation is plastic, the remainder of the deformation is elastic [25]. Thus, due to elastic recovery, relatively large reductions in F can occur with little increase in interface resistance if the interface is undisturbed.

The ability of an electrical contact to maintain a stable interface resistance depends on the degree of plastic deformation and also on the amount of elastic recovery present for individual asperities. The amount of plastic deformation and elastic recovery must vary for each asperity since the original separation distances between asperity pairs are different [26], [27]. Therefore, not all asperities break at once. Since the interface resistance is based on the resistance of each asperity acting with the resistances of all other asperities in some series/parallel combination, many asperities can fail before a significant change in resistance is seen.

Stress relaxation is intrinsic to any metal under load. The main contributing factors to the rate of stress relaxation over time are the resistance to stress relaxation of the alloy used for the contact spring and the temperature to which the contact is subjected. Stress relaxation can accelerate rapidly with increased temperature. Tests have been performed on mated contact pairs to simulate field use over time to evaluate the effect of stress relaxation on interface resistance. Figure 4 shows the loss of normal force for three groups of a specific connector type with each group exposed to a different temperature for 200 days [28]. The near-parallel lines of percent reduction in normal force, which correlates directly to reduction in stress, when plotted on a log-linear scale, are typical of an Arrhenius relationship expected for stress relaxation [28]. Note that the rate of stress relaxation is rapid early in the exposure but declines over time. The exposure temperatures used in the test which provided the data in Fig. 4 are typical of the conditions of actual use of many connectors.

Figure 5 shows the effect that a reduction in F can have on the interface resistance of electrical contacts of the same type as those used in the tests that provided the data in Fig. 4. The contacts were checked for interface resistance change periodically. What is of interest is that despite the reduction in normal force of the contacts during the initial 182 days of exposure, there was negligible change in the interface resistance. During this period, the contacts had not been unmated. However, on the 182nd day, immediately after

the interface resistances were measured, the connectors were unmated and remated, and the interface resistances were measured again. It was at this point that larger changes in interface resistance occurred with the largest change being for the connectors exposed at the highest temperature. The reason for this is that, as explained above, the loss of normal force may not directly cause a significant reduction in the number and size of the asperities due to elastic recovery at asperity-asperity interfaces. But when the connectors were unmated and remated, new asperities were created at the now lower normal force and thus per (2) would have a higher interface resistance [29].

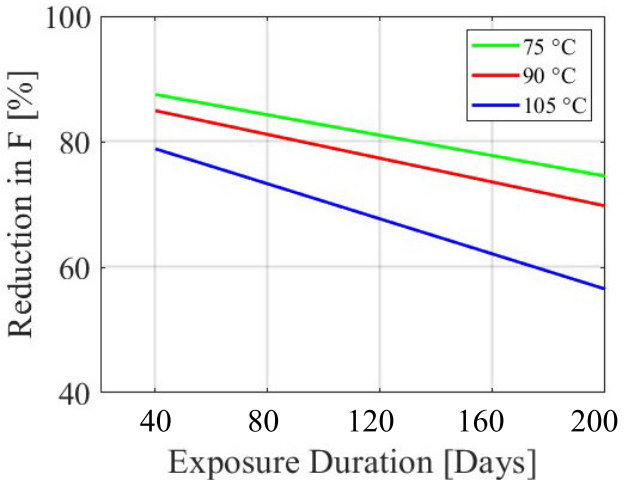

FIGURE 4. Stress relaxation study on phosphorus-bromine contacts showing contact normal force F at three different temperatures.

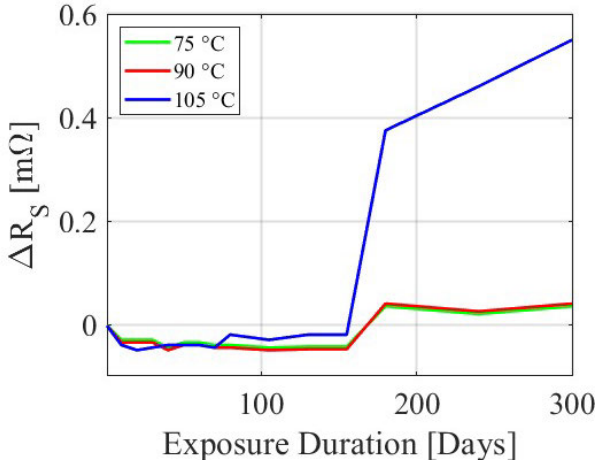

FIGURE 5. Heat age testing with cycling at three different temperatures showing how R_S changes with time.

Thus, stress relaxation by itself will not necessarily result in an increase in interface resistance. However, it will reduce frictional forces at the interface. This will reduce the stability of the interface making it more likely to move. Under these conditions, stresses such as vibration and temperature cycling at levels which would not result in increased interface resistance in a new connector may cause increases as the connector ages.

C. THE IMPACT OF WEAR ON ELECTRICAL CONTACTS

It was mentioned at the beginning of Sec. II that most connector electrical contacts use a plating system consisting of a thin layer of one or more metals deposited over the contact base metal. These plating systems are designed to optimize electrical performance of the contact surfaces to both minimize the initial interface resistance and to maintain a low interface resistance under normal conditions. Degradation of the plating system during the life of the connector can lead to failure. The plating material can be displaced and/or lost if wear due to relative motion between the contact surfaces occurs. The end result of the loss of plating material is an increase in R_S. The primary causes of wear include vibration, temperature cycling (due to expansion and contraction of the contacts), and a high number of mating cycles. As the various types of motions increase, the degree of contact wear typically increases.

The plating systems chosen for a specific connector will, in part, take the issue of contact wear into consideration. For example, a connector which will be subjected to only a few mating cycles during its lifetime and used in applications with limited vibration and temperature cycling may have a soft plating such as tin or silver plating. Being relatively soft materials, tin or silver tend to create a larger area of metal-to-metal contact for a given normal force. Connectors that are designed to undergo hundreds or thousands of mating cycles, either because of operation in high-vibration environments or because they will be subjected to many large temperature excursions, will have hard plating of, e.g., cobalt-hardened gold or palladium-nickel alloy. Most contact plating systems usually have an *underplating* of nickel to reduce the rate of wear if some sections of the upper plating wear into the surface of the nickel underplating.

Since contact platings are specifically applied for their ability to maximize the electrical performance of the electrical contact interface, the loss of plating material due to wear can lead to failure. With the plating system degraded, the asperities that were originally created on the electrical contact surface will be replaced by new asperities on the underplating or even the contact base metal. For electrical contacts plated with materials such as tin or silver, since the underplating and the contact base metal are harder than the tin or silver, then by (2) R_S will increase. In the case of gold and palladium platings, the underplating may have similar hardness, but being a non-noble metal, it may develop a hard non-conductive oxide layer which increases R_S.

Even connectors that are designed to undergo hundreds or thousands of mating cycles will eventually fail due to wear [30], [31] if operated beyond their design life. Consider the Lightning Bolt connector at the beginning of its life cycle in Fig. 6a. All the gold plating material is on the contact surface with no signs of wear. As time goes on, and as the

connector undergoes field use, this plating material wears off, as shown in Fig. 6b, and causes R_S to increase.

In the case of connector applications with few mating cycles, wear can still occur due to vibration. It is not necessary for the wear to penetrate through the surface plating. Non-noble platings such as tin are susceptible to *fretting* corrosion. Small-amplitude contact interface motion in the range of 0.05 mm can displace the tin asperities, thereby exposing the tin to air leading to rapid oxidation. The resulting tin-oxide particles are non-conductive and hard; over many vibration cycles or temperature changes, these particles can build up and lead to electrical contact failure. This failure may be complete or may be in the form of microsecond-level electrical discontinuities. Electrical contacts can often operate without failure when subjected to one stress or another but will fail when subjected to multiple stresses simultaneously.

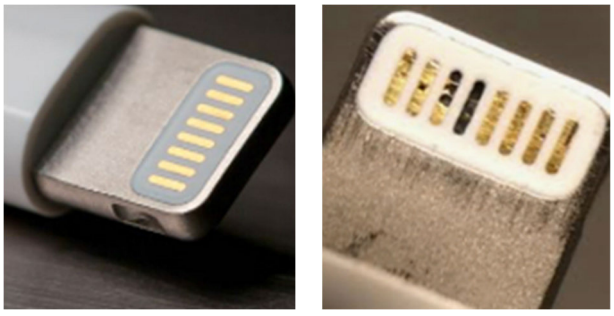

(a) (b)

FIGURE 6. Electrical contact plating (a) on a new connector and (b) on a well-used connector from continuous in-field use.

Figure 7 shows an example of this behavior [28]. For this figure, the test combined vibrations and exposure to elevated temperature. The vibrations were performed along three translational axes and three rotational axes simultaneously, with a random temporal profile. The test started with temperature near the room temperature and 10 G_{rms} of vibration total across all vibration axes. The vibration was stepped up to 20 G_{rms} after 6 min, and to 30 G_{rms} after another 6 min, returning to 10 G_{rms} in the 18th minute. The temperature was then increased to 60°C and the 10-20-30-10 G_{rms} vibration cycle was implemented thereafter. At the conclusion of the second vibration cycle, the temperature was raised to 90°C and the 10-20-30-10 G_{rms} vibration cycle was repeated a final time.

Electrical discontinuities of a micro-second or longer are indicated in Fig. 7 by yellow spikes. No discontinuities were detected at any of the vibration levels at room temperature. The first discontinuities were observed at the highest vibration level during the mid-range temperature phase of 60 °C. During the final phase of the test at 90 °C, discontinuities occurred at both the 20 G_{rms} and 30 G_{rms} vibration levels. Accordingly, it can be concluded that disturbances such as vibrations can engender discontinuities

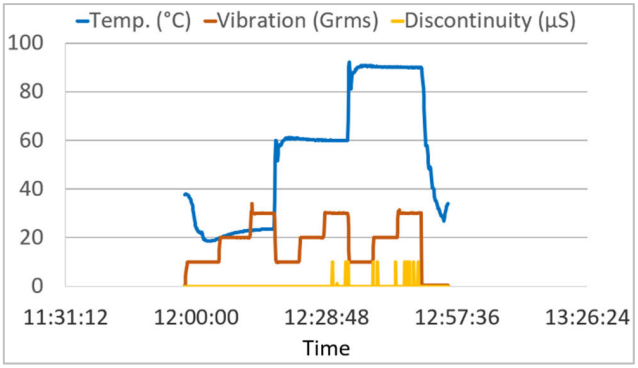

FIGURE 7. Temporal profiles of temperature, vibration, and discontinuity demonstrating how vibration and temperature can disrupt the electrical performance in connectors.

in electrical contacts, with operating conditions playing a major role.

D. THE CAUSES AND EFFECTS OF CORROSION

Another common connector failure mode is corrosion. Figure 8 shows what corrosion can look like on exposed metallic contacts. There are different types of corrosion and all of them are generally non-conductive. Because corrosion products are non-conductive, they have a negative impact on electrical performance by increasing R_S.

There are various sources of corrosion which must be managed to maintain an acceptable resistance across a contact interface. Methods of mitigating corrosion include the use of appropriate plating systems such as noble metals like gold or palladium for applications involving exposure to pollutant gasses and nickel for acidic applications such as battery connectors. It is also common to use contact lubricants and connector housings to prevent ingress of corrosion elements.

Another type of corrosion is fretting corrosion. It often occurs in non-noble metals, when mated contacts have repeated small movements or micro-motions relative to each other such as from repeated expansion and contraction due to temperature cycles or vibration. These micro-motion cycles can expose asperities, which are normally airtight, and allow the newly exposed electrical contact surface to oxidize. Over many micro-motion cycles, the oxide particulates build up in the electrical contact interface and may eventually cause the contacts to fail. Common mitigation methods for fretting corrosion include the use of normal forces of sufficient magnitude to prevent micro-motions. Lubricants are also commonly used to prevent exposure of electrical contacts to oxygen or other corrosive gasses that may be in the environment.

A phenomenon known as *super-temperature*, commonly seen in power connectors, is also known to cause corrosion. Since power connectors carry higher electrical currents, they tend to operate at higher temperatures, about 30 °C above the ambient temperature. At these elevated temperatures, the asperities within the power contacts, being very small,

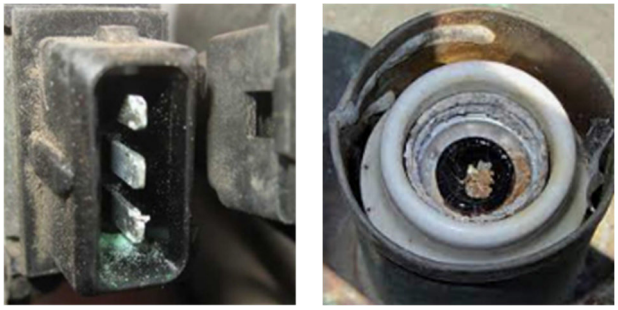

(a) (b)

FIGURE 8. Corrosion built up on (a) a power connector and (b) an electrical light socket due to open exposure to the elements.

have current densities leading to very high local temperatures which can cause rapid oxidation. Mitigating these effects typically requires the use of a high normal force on the contact so that the number and size of the asperities is increased in order to decrease the current density. A higher normal force also helps in preventing motion at the contact interface.

III. BRIEF HISTORY OF WIRELESS POWER TRANSFER

As is clear from Section II, electrical contacts have many potential failure modes that can be traced back to a single cause: exposed metallic contacts. *The best way to eliminate these failure modes in connectors is to eliminate metallic contacts completely.* The non-metallic connector (NMC) does exactly this. And it does that by using the methods of wireless power transfer (WPT) which has become technically feasible only recently. This section explores the reasons why.

A. THE DISCOVERY AND EXPERIMENTAL VALIDATION OF WIRELESS POWER TRANSFER

The first two decades of the 21st century were a time of rebirth for the field of WPT and its applications. While the theoretical fundamentals of WPT had been firmly established by Maxwell before 1873 [32], with a major contribution from Poynting in 1884 [33], WPT remained technically infeasible for the remainder of the 19th century and most of the 20th century.

The theoretical foundations of electromagnetic wave propagation in free space from a transmitter to a receiver were experimentally validated by Hertz in 1888 using the 450-MHz oscillator shown in Fig. 9 [34]. Shortly thereafter, Tesla and Marconi came up with the first WPT applications. Whereas Tesla transmitted high power with a 150 kHz carrier wave in 1890, Marconi transmitted signals with a 250 MHz carrier wave in 1895 [35], [36], [37], [38]. However, Tesla's equipment received a small fraction of the power transmitted because of the low directivity of his transmitter. Furthermore, the low operating frequency corresponded to an extremely large free-space wavelength and required the use of physically large components [39], [40], [41] unsuitable for WPT applications.

At the start of the Second World War, there came an urgency for better radio communication and radar systems which, in turn, gave incentives to develop robust microwave WPT (MWPT) systems. The 35 years that followed saw significant breakthroughs in the subsystems required to make up a complete MWPT system. It was also during this period that MWPT applications became possible for space exploration. The late 1980s and early 1990s saw an acceleration in semiconductor technology that helped to surmount some limitations and brought in the next wave of WPT innovation, but this time it was for applications that would be classified as non-radiative in the near zone and eventually give way to the various types of WPT technologies in widespread use today that are impacting multiple industries.

There are several reasons why it took an entire century for WPT to evolve into its current state with a seemingly endless potential for applications. The three main factors that limit WPT applications are: (i) the transmitting and receiving power-conversion methods, (ii) the physical sizes and weights of the transmitting and receiving antenna systems, and (iii) the inefficiencies of both [42], [43], [44].

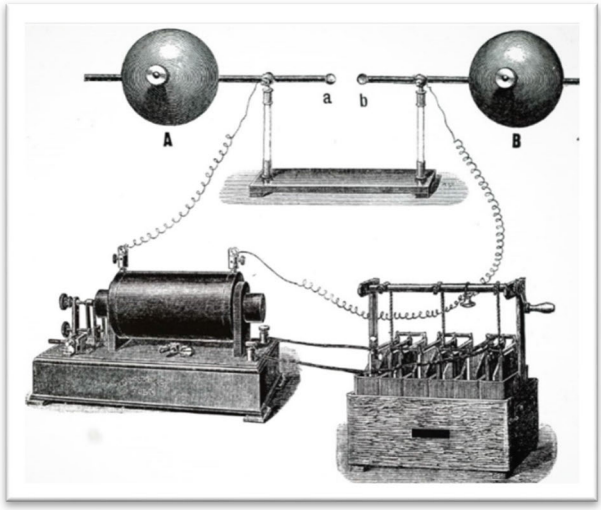

FIGURE 9. Illustration of Hertz oscillator, the first experimental demonstration of wireless power transfer. [Image license GettyImages-921869042].

B. THE FIRST COMMERCIAL APPLICATIONS OF MWPT

The first breakthrough that eventually helped overcome the physical limitations arising from low operational frequencies took place at Stanford University in 1937 with the invention of the klystron by the Varian brothers [45]. The vacuum diode had been invented in 1904 by Fleming and the triode in 1906 by De Forest, but both had significant power and efficiency limitations. With a power-handling capability several orders of magnitude higher relative to the vacuum diodes and triodes [46], the klystron was the first vacuum tube used in radar, radio communication systems, and linear

particle accelerators. In addition, klystrons were able to operate at much higher frequencies from UHF onwards.

The magnetron, invented in 1940 at the University of Birmingham by John Randall and Harry Boot, was significantly smaller than the klystron [47]. Additionally, the magnetron permitted operational frequencies well within the ISM band of 2.4-2.5 GHz. However, there still was no efficient way to convert the received power in MWPT systems into DC, as is common today in both radiative MWPT applications in the far zone and non-radiative WPT systems in the near zone [42], [48], [49], [50].

The space race during the beginning of the Cold War between USA and the USSR in the 1950s gave impetus for new MWPT applications. Advances in vacuum-tube technology eventually enabled MWPT power transmission, a development led by organizations such as the Raytheon Company, the Marshall Space Flight Center at NASA, and the Jet Propulsion Laboratory, funded by the U.S. Department of Defense [51]. The primary applications of interest were robotic space probes, solar-powered satellites, ballistic missile systems, microwave-powered helicopters, and microwave power transmission from solar-powered satellites to earth [52], [53], [54]. However, in the early years, the physical size, weight, and efficiency of vacuum tubes began to play larger roles for technical feasibility over the physical size of antennas.

A breakthrough in technical feasibility for MWPT came in the 1960s with the emergence of the much smaller rectifier diodes made of semiconductors. The original rectifier diodes were demonstrated [50] to work in a rectenna design of 28 half-wave dipole antennas that were each terminated with a full bridge rectifier using point-contact rectifier diodes. With these diodes, the power- handling capacity of the original rectenna system reached 7 W, with reported collection and power conversion efficiencies (PCE) between 40% and 50%. While this experiment proved to be a significant breakthrough in size reduction for MWPT systems, they needed to be made more energy efficient; also, the power density needed to be higher for the concept to be extended to more applications. This improvement came in the form of Type-2900 Schottky-barrier diodes, which significantly increased efficiency with lower capacitance, higher switching speeds, and power-handling capability [55]. The development of Type-2900 Schottky-barrier diodes is what eventually gave rise to modern WPT systems that are used today.

C. THE DEMAND FOR A NEW WPT SYSTEM

From the early 1970s to the late 1990s, improvements in size reduction, operational frequency, and power-conversion efficiency became dependent on advances in semiconductor technology. The interest and demand for a different kind of WPT system besides MWPT systems arose that was based on inductive coupling [56] in the near zone. Proposals for dynamic charging of electric vehicles were introduced as early as the 1970s [56], [57]. By the 1990s, proposals for the first wireless charging devices for consumer electronics, as we know them today, began to be introduced [58], [59], [60].

It was also during the 1990s that 3- and 4-axis robotics dominated automobile-manufacturing assembly lines. The cabling used in these robotic systems would often experience mechanical strain, leading to bent and broken connector pins. Therefore, proposals were made for WPT (i.e., cableless) systems that could transfer both power and signals over a coupler for cableless motor drive systems [61], [62], [63], [64], [65]. High-power inductive power transfer (IPT) systems for robotic systems were operated at 25 kHz and 650 V by the early 1990s.

Contemporaneously, significant breakthroughs in inverter and rectifier architectures, circuit designs, and device physics were made. The resulting improvements in power-conversion efficiency gave way to the WPT revolution [66], [67], [68], [69], [70], [71], [72], [73], whose salient features have been reviewed extensively [44], [74], [75], [76], [77], [78], [79], [80], [81], [82], [83], [84]. These review papers all confirm that the technical feasibility of WPT has been limited from the time of Hertz and Tesla by the physical sizes of the transmitting and receiving coils, the physical size and weight of power-electronic devices, the efficiencies of both, and the operational frequency. The technical breakthroughs over time that have improved these areas has given way to new WPT applications that is a trend that continues today.

Not coincidentally, from the early 2000s, efforts to standardize WPT systems began to be made by the Wireless Power Consortium, IEEE, and other organizations, aimed at ensuring device compatibility and addressing public safety concerns regarding electromagnetic exposure [85].

D. THE CONVENTIONAL WPT CLASSIFICATION

WPT has been classified into two main types: near zone and far zone. The delineation of the two zones depends on the free-space wavelength λ and the size of the transmitter, because both determine the transfer distance that the electromagnetic wave travels from the transmitter [49], [86], [87], [88]. Near-zone WPT is commonly split into two subtypes: radiative and reactive (or non-radiative).

It has become common in WPT literature to classify the transfer modes as short-range, mid-range, and long-range, from the range r as the radial separation distance between the transmitter and the receiver. With D_{out} as the diameter of the transmitter's aperture, the short range is confined to the near zone $r < r_S$, where

$$r_S = 0.62\sqrt{\frac{D_{out}^3}{\lambda}}. \tag{3}$$

The long range extends throughout the Fraunhofer zone $r > r_L$, where

$$r_L = \frac{2D_{out}^2}{\lambda}. \tag{4}$$

Between these two zones lies the Fresnel zone $r_S < r < r_L$ [86], wherein mid-range WPT is taken to occur.

The three zones are illustrated in Fig. 10 and a high-level WPT hierarchy is illustrated in Fig. 11. Both signal-transfer and power-transfer WPT are categorized in the WPT hierarchy. Prior to the 1980s, nearly all of the MWPT applications operated in the Fraunhofer zone. The industry demand for a new WPT system for robotics applications and electric vehicles are examples of WPT applications that operate in the near zone. The Fresnel zone began to be considered from 2000 onwards.

Today, wireless charging for electric vehicles, and consumer electronics applications (such as ear buds, digital watches, and smartphones), biomedical applications and many others dominate in the near zone. IPT is mostly used for these applications but it is also common for capacitive power transfer (CPT) to be used for both signal and power transfer without cabled connections [89].

Due to technical progress during the 1990s, new multi-coiled magnetic resonance WPT systems were introduced in the early 2000s to efficiently transfer higher power levels over larger distances [90], e.g., transferring 120 W of power over 2.5 m to power a lightbulb [91]. Metamaterials also were introduced and came to be used to improve WPT efficiency in new ways [92]. Communication protocols such as USB, Wi-Fi, Bluetooth, ultra-wide band (UWB) transmission, etc. have also been developed and are widely used for signal transfer in many digital devices today [93].

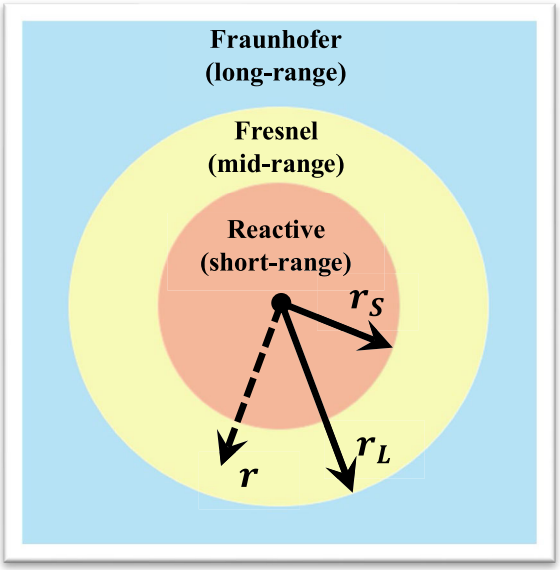

FIGURE 10. Illustration of the three field regions in WPT. Given a fixed transmitting outer coupler diameter D_{out}^{Tx}, the wavelength λ determines the field region the system will operate in.

As the historical trends show, technical breakthroughs in different industries have often laid the foundations for breakthroughs for new technologies in both technical and economic feasibility. This section demonstrated how this has happened for the field of WPT. Yet, as explicated in Section I the connector industry has remained largely untouched in the way they connect devices together by using electrical contacts. As explicated in Section II, electrical contacts have many failure modes. Sections IV and V shows how this situation can be improved for both signal transfer and power transfer NMCs, respectively.

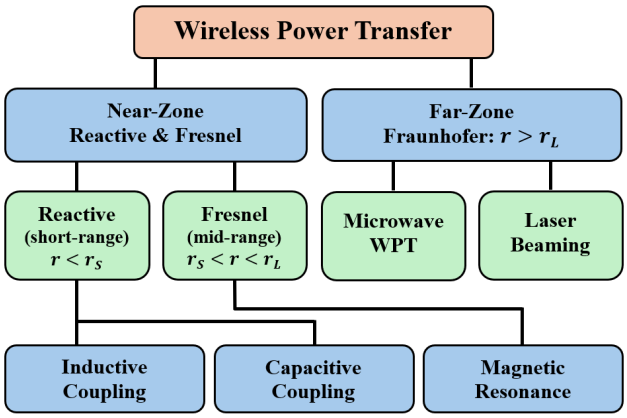

FIGURE 11. Illustration of the conventional WPT hierarchy showing the classification criteria of near-zone and far-zone WPT technology.

IV. SIGNAL TRANSFER THROUGH NON-METALLIC CONNECTORS

Electrical contacts have overwhelmingly dominated the connector industry for some 150 years, even though they are plagued by diverse performance problems, often to the point of failure, necessitating high monetary expenses to maintain, avoid, and rectify. Additionally, these types of efforts are deleterious to the ecosystem [94].

As discussed in Section III, much progress has occurred over the last two decades in WPT where it is now advanced enough to be applied as a replacement for electrical contacts, and the NMC era can be ushered in.

The NMC concept for signal transfer is introduced here and applied to the USB flash drive. The USB flash drive is a consumer-electronics device that undergoes multiple insertion cycles and routinely suffers from wear and corrosion, as illustrated in Fig. 6. The NMC-based USB concept envisages a hermetically sealed waterproof interface that is corrosion free and, therefore, can withstand an unlimited number of insertion cycles — an outstanding benefit of the NMC concept.

A. HIGH-SPEED SIGNAL TRANSFER NMCs

Too many different kinds of high-speed connectors exist to be listed here, Ethernet and USB operating at speeds up to 10 Gbps and 40 Gbps, respectively, being two ubiquitous examples. At such high data-transfer rates, several deleterious factors such as signal reflections, near-end cross talk, and bit error rates, must be considered in the context of signal integrity.

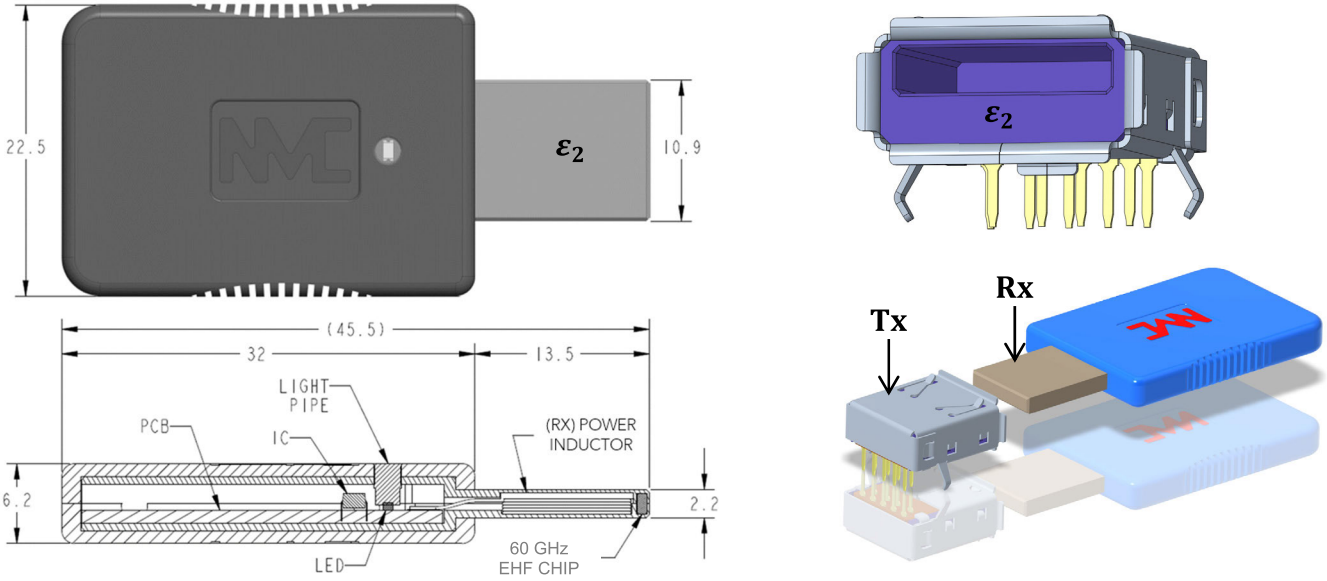

FIGURE 12. Illustration of how the NMC concept is applied to the USB flash drive application using EHF for high-speed data transfer and IPT for power transfer.

Connectors create a break in an otherwise continuous electrical pathway and ultimately impacts the rise time of the signal according to [95]

$$RT_{out}^2 = RT_{in}^2 + RT_{intc}^2. \tag{5}$$

Here, RT_{out} is the rise time of the output signal, RT_{in} is the rise time of the input signal, and RT_{intc} is the rise time intrinsic to the connector. No matter how well engineered a connector might be, RT_{intc} will always exist and increase RT_{out}. As a consequence, the bandwidth

$$BW \approx \frac{0.35}{RT_{out}} \tag{6}$$

will be reduced.

By eliminating connector failure modes by using NMC, either with inductive or capacitive coupling methods [96], [97], [98], [99], [100] or by repurposing extremely high frequency (EHF, $f \in [30, 300]$ GHz) radio technology with a system-on-a-chip antenna [101], [102], [103], [104], the bandwidth can be significantly improved. The latter strategy has shown to be superior to the former for three reasons. First, IPT limits the operational frequency due to the skin and proximity effects by increasing the effective impedance of an inductor coil at higher frequencies [105]. The second reason arises from limitations on the switching speed of MOSFETs used in conventional WPT inverter and rectifier architectures. The third reason is the proven extremely low latency of EHF technology and the significant energy savings in comparison to other methods.

To buttress the third reason, Table 1 compares the measured Upload/Download performance of common wireless protocols by testing the effective data rate, power consumption, the time to transfer 1 GB of data, and battery consumption. These data demonstrate the low latency of EHF technology relative to other common wireless technologies. Table 1 makes it clear that EHF technology delivers an effective data transfer rate 16 times faster than ultrawideband (UWB) technology, consumes six times less power, can transfer 1 GB of data 32 times faster, and has five times less impact on battery consumption. EHF technology is also superior to long-term evolution (LTE) and Wi-Fi technologies. For these reasons, the EHF technology is very appropriate for high-speed signal-transfer NMCs.

TABLE 1. Comparison of common WPT technologies on performance for data upload / download transfer.

Method	Data Rate (Gbps)	Power (Watts)	1 GB Transfer (seconds)	Battery Cons.
EHF	4 / 4	0.05 / 0.05	2 / 2	<0.01% / 0.01%
LTE	0.005 / 0.02	3.4 / 2	1,600 / 400	27.7% / 4.08%
Wi-Fi	0.02 / 0.04	1.5 / 2	400 / 200	3.06% / 2.04%
UWB	0.25 / 0.25	0.3 / 0.3	32 / 32	0.05% / 0.05%

B. FIELD ZONES FOR HIGH-SPEED NMCs

Common WPT-enabled devices such as cellphone chargers, smart toothbrush chargers, and smart watches provide multiple degrees of freedom in physical space for the design of Tx-Rx coil pairs. This is not the case for NMCs, for which the form factor is constrained to which the WPT system must be made to fit. Hence, the EHF technology must be adopted for high-speed signal transfer NMCs in preference to IPT and CPT.

To illustrate this important point, consider the application of the NMC concept to a USB flash drive shown in Fig. 12. The USB 4.2 operates at a data rate of 120 Gbps and can simultaneously deliver 100 W power. While it is possible to support both power transfer and signal transfer over the same inductive interface [105], that is not true at the high data transfer rates that USB 4.2 must deliver. Power transfer and high-speed signal transfer must happen separately, as shown in drawing in Fig. 12 with the 60 GHz EHF chip positioned in towards the front and the power inductor behind the chip. The Rx power inductor occupies most of the physical space and it must also comply with the Qi2 standard at 150 kHz for power transfer. Therefore, the Rx diameter is very small for high-speed signal transfer and the 60 GHz EHF chip is positioned at the very front of the USB plug.

When inserted into a USB Type-A receptacle, the Rx chip is coaxial with the Tx chip. Both Tx and Rx are encapsulated with a polymer of relative permittivity ε_2. Also, both Tx and Rx silicon-on-chip antennas are encapsulated by silicon of relative permittivity $\varepsilon_1 = 11.7$, as shown in Fig. 13(a), and the Rx and Tx are separated by a gap g when the plug is inserted into the receptacle. Figure 13(b) shows how the EHF chips are mounted onto a PCB substrate.

In addition to a small form factor, the field zone (Fig. 10) must be considered in order to define the power-transfer efficiency (PTE), which depends on the data transfer rate and system operating frequency. To illustrate this point, outer diameter of the transmitting antenna aperture, D_{out}^{Tx}, is plotted in Fig. 14 as a function of r_s and r_L from (3) and (4). In practical situations, $g \leq 1$ cm. With fixed λ and D_{out}^{Tx}, it is possible that $r_L \gtrless r_s$ and the design equations stemming from PTE for signal transfer will change whether $g \gtrless r_s$ or $g \gtrless r_L$ or $r_s \gtrless g \gtrless r_L$.

C. NMCs IN THE FAR-ZONE

To find PTE at fixed λ when g lies in the Fraunhofer zone and the apertures are assumed to be coaxial, the Friss transmission equation [106]

$$PTE = \frac{P_{Rx}}{P_{Tx}} = e_{Tx} e_{Rx} \frac{\lambda^2 D_{out}^{Tx} D_{out}^{Rx}}{(4\pi g)^2} \tag{7}$$

must be used. Here, P_{Tx} and P_{Rx} are the transmitted power and received power, respectively; e_{Tx} and e_{Rx} are the radiation efficiencies of the Tx and Rx antennas, respectively; and D_{out}^{Tx} and D_{out}^{Rx} are the outer diameters of the Tx and Rx antenna apertures, respectively. Incorporating Γ_{Tx} and Γ_{Rx} as the complex-valued reflection coefficients in the circuitries of the Tx and Rx antennas, respectively, (7) becomes

$$PTE = e_{Tx} e_{Rx} \left(1 - |\Gamma_{Tx}|^2\right) \left(1 - |\Gamma_{Rx}|^2\right) \frac{\lambda^2 D_{out}^{Tx} D_{out}^{Rx}}{(4\pi g)^2}. \tag{8}$$

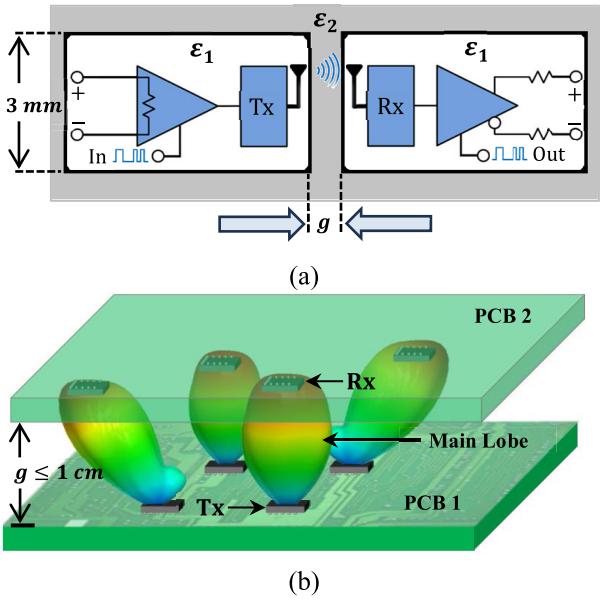

FIGURE 13. (a) NMC_{EHF} diagram showing input modulated signal being transmitted over an air gap g and (b) the small size of the Tx-Rx EHF chips.

In terms of antenna gains $G_{Tx} = e_{Tx}\left(1 - |\Gamma_{Tx}|^2\right) D_{out}^{Tx}$ and $G_{Rx} = e_{Rx}\left(1 - |\Gamma_{Rx}|^2\right) D_{out}^{Rx}$, (8) can be rewritten as

$$PTE = G_{Tx} G_{Rx} \left(\frac{\lambda}{4\pi g}\right)^2. \tag{9}$$

Equations (7) and (8) show the dependence of PTE on the size of antenna apertures. Physical space is limited in NMC applications so that D_{out}^{Tx} and D_{out}^{Rx} are very small, and other parameters will need to be adjusted in order to maximize PTE. With λ and g also very small, NMC operation will typically depend on G_{Tx} and G_{Rx} for optimal PTE. Therefore, due to the very low latency of antenna circuitry in the EHF band, EHF is preferable to UWB and other lower-frequency technologies.

The Friss transmission equations (7)–(9) assume that electromagnetic waves between the two antennas are propagating in unobstructed free space and that the operational polarization states of both antennas are the same. Furthermore, (7)–(9) only apply when $g > r_L$ (i.e., the NMC system operates in the far zone).

For the Ethernet application where the operational frequency $f = 5$ GHz (10 Gbps), which lies within the UWB range, the NMC system will operate in the far zone for $D_{out}^{Tx} < 5.76$ mm. As illustrated in Fig. 14 there will be a transition from the far zone to the near zone as D_{out}^{Tx} increases beyond 5.76 mm.

D. NMCs IN THE NEAR-ZONE

Since the USB 4.2 in Fig. 12 operates at $f = 60$ GHz (120 Gbps) and since the NMC is physically restricted to $D_{out}^{Tx} < 3$ mm and $g \leq 1$ cm as shown in Figs. 13(a) and 13(b), respectively, the NMC will not operate in the far zone. Instead, it will operate in the near zone and be reactive,

as illustrated in Fig. 15. In this case the transition between the near and the far zones takes place at $D_{out}^{Tx} = 0.01$ mm. Moreover, the electromagnetic waves will not propagate in unobstructed free space because the dielectric material with relative permittivity ε_2 will create signal reflections. For these reasons, the Friis transmission equations (7)–(9) do not apply, and a new model is needed to better describe PTE.

Figure 16 shows a plot of D_{out}^{Tx} vs. f when the Fresnel region in Fig. 10 is absent, i.e., $r_S = r_L$. In that case, (3) and (4) yield

$$D_{out}^{Tx} = \frac{0.0961\, c}{f}, \tag{10}$$

where c is the speed of light in free space.

A better way to model the scenario in Fig. 13(a) for determining the PTE in the near zone is with a dielectric multilayer. Figures 17(a)-(c) represent a model of Fig. 13(a) where both Tx and Rx antennas are encapsulated in silicon chips (so that $\varepsilon_1 = \varepsilon_{Si}$), each chip fronted by a polymer slab with relative permittivity ε_2 and thickness $d/2$ such that $g \geq d$. When the USB receptacle and plug are mated, as shown in Fig. 17(b), the Tx antenna is switched on. Maximum power transfer requires that

$$\left|\Gamma_{12} + \Gamma_{21} e^{-j2\beta_2 d}\right| = 0, \tag{11}$$

where $\Gamma_{12} = -\Gamma_{21} = (\eta_2 - \eta_1)/(\eta_2 + \eta_1)$, $\eta_1 = \eta_o/\sqrt{\varepsilon}_1$, $\eta_2 = \eta_o/\sqrt{\varepsilon}_2$, $\beta_2 = 2\pi\sqrt{\varepsilon}_2/\lambda$ and η_o is the intrinsic impedance of free space [107]. Equation (11) simplifies to

$$|\Gamma_{12}|\left|1 - e^{-j2\beta_2 d}\right| = 0. \tag{12}$$

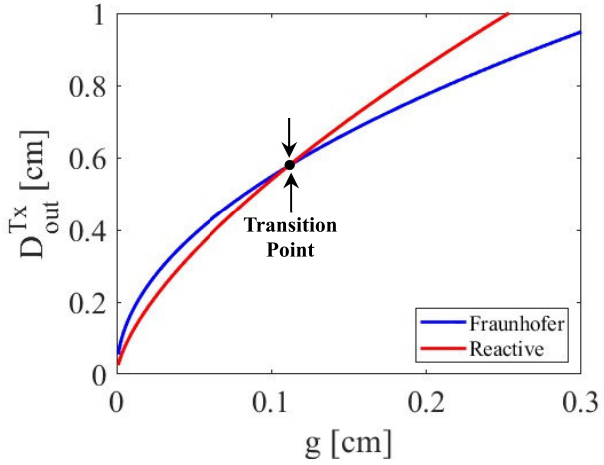

FIGURE 14. Near-zone (2) and far-zone (3) approximations at $f = 5$GHz within the UWB band showing field transition at $\left(g, D_{out}^{Tx}\right) = (1.10, 5.76)$ mm.

By Euler's formula, the condition (12) requires that

$$d = \frac{m}{2}\frac{c}{f\sqrt{\varepsilon_2}}, m \in \{1, 2, 3, \ldots\}. \tag{13}$$

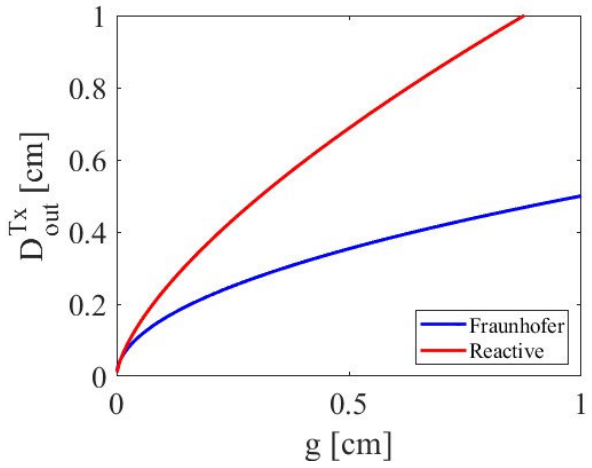

FIGURE 15. Near-zone (2) and far-zone (3) approximations at $f = 60$GHz within the EHF band showing field transition at $\left(g, D_{out}^{Tx}\right) = (0.48, 0.01)$ mm.

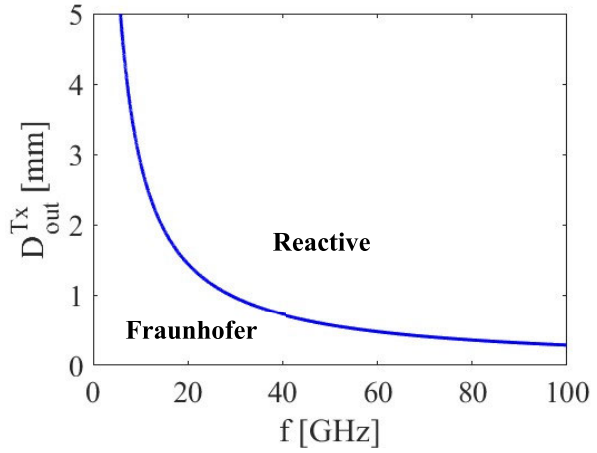

FIGURE 16. Boundary between far-zone and near-zone after plotting (9) for D_{out}^{Tx} as a function of operational frequency f.

Provided that ε_2 is purely real and positive, the smallest value of d is

$$\min\{d\} = \frac{c}{2f\sqrt{\varepsilon_2}}. \tag{14}$$

Equation (14) suggests that both f and ε_2 should be as large as practicable. The minimum value of d as a function of ε_2 is plotted in Fig. 18 for $f \in \{30, 45, 60\}$ GHz, showing that a range of dielectric materials can be used and that there is greater choice of materials in the low-frequency portion of the EHF band.

Provided (12) holds, PTE = 1. In practice, that will not be true because of (i) variations in material quality from lot to lot [108], (ii) manufacturing imperfections [109], (iii) temperature fluctuation [110], and (iv) contamination of contact surfaces by particulate materials in the environment [111]. Corrosion during use is not a significant issue because the plug and receptacle are hermetically sealed, as indicated in Fig. 12.

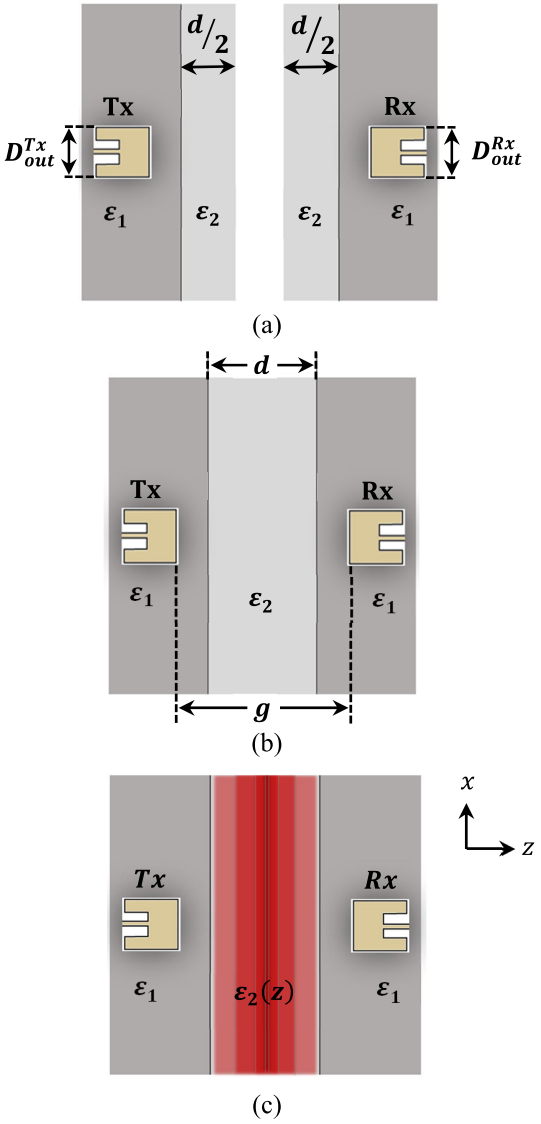

FIGURE 17. Model of the NMC in Fig. 13(a) showing both Tx and Rx antennas encapsulated by silicon of relative permittivity ε_1 that is also encapsulated by a polymer of relative permittivity ε_2 of thickness d. Conditions for (a) unmated, (b) mated, and (c) mated contamination with changing dielectric $\varepsilon_2(z)$.

In case that significant deformations and contamination occur, the gap g may have to modeled as a multilayered region with layers of thickness on the order of $\frac{c}{10f\sqrt{|\varepsilon_2(z)|}}$ with piecewise uniform $\varepsilon_2(z)$ as shown in Fig. 17(c), in order to determine PTE. For the details, the reader is referred to a textbook [112].

This section demonstrated that the spatial zone – reactive, Fresnel, or Fraunhofer – in which a WPT system operates determines how PTE should be calculated. For WPT over small distances, and in NMCs, D_{out}^{Tx} and D_{out}^{Rx} are typically 3 mm or less. The classification of the gap g will change from the near zone to the far zone, or vice versa, if the communication protocol (e.g, UWB and EHF) is changed. Therefore, NMCs must be distinguished from other WPT

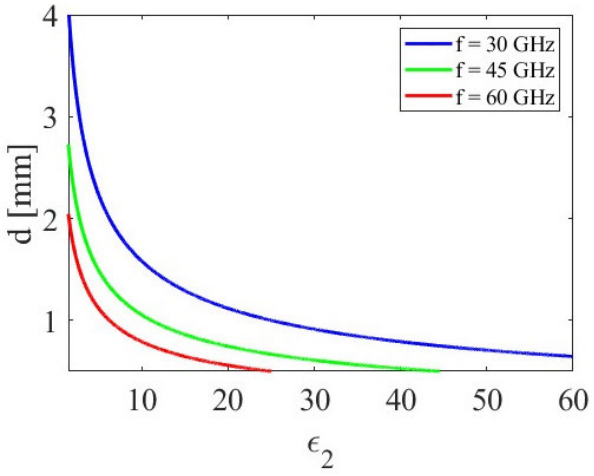

FIGURE 18. Optimized value of d as a function of the relative permittivity of ε_2 for several values of f within the EHF band.

systems. A new category WPT, called μWPT, must be created to accommodate NMCs. The WPT hierarchy shown in Fig. 11 must be modifed to the one shown in Fig. 19.

V. POWER TRANSFER THROUGH NON-METALLIC CONNECTORS

There are four categories of WPT systems in the near zone, depending on the number of inputs that supply power on the Tx side and the number of outputs that receive power on the Rx side. These categories are commonly referred to single-input-single-output (SISO), multiple-input-single output (MISO), single-input-multiple-output (SIMO), and multi-input-multi-output (MIMO) [84].

The most common category of NMC applications is SISO, due to limitations on space. Applications include charging devices in consumer electronics, household kitchen appliances, biomedical applications, and EV charging stations, in order to eliminate wires and cables and improve convenience for end users [113]. This section concentrates on power transfer for NMCs, introduces applicable circuit topologies, and presents ways to improve the PTE and power density.

A. POWER TRANSFER MODALITIES FOR NMCS

There are two modalities of WPT for power transfer in the reactive zone classified as either inductive power transfer (IPT) or capacitive power transfer (CPT). There are advantages and disadvantages in both and the modality that ends up being used depends on the application [44], [81], [89], [114], [115].

Both reactive modalities of WPT use the same basic setup, as shown in Figs. 20(a) and (b). Each modality comprises the following four devices: a DC voltage V_{IN} is fed to (i) a controller that implements a pre-programmed timing sequence to create an AC waveform that is sent to (ii) a power inverter-amplifier. The amplified AC waveform passes through (iii) a primary circuit for which multiple choices

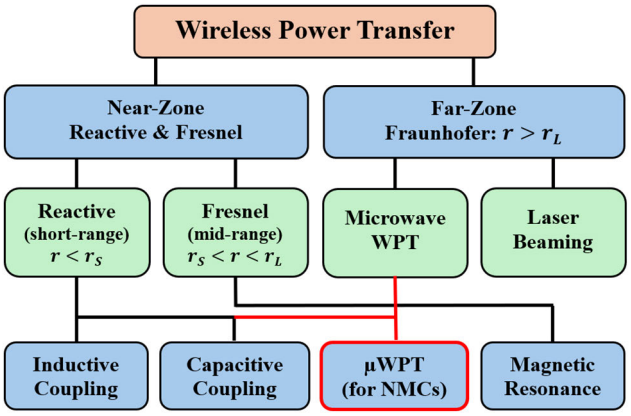

FIGURE 19. Proposed new WPT hierarchy showing the inclusion of μWPT as either near-zone or far-zone WPT technology with a small Tx-Rx separation distance.

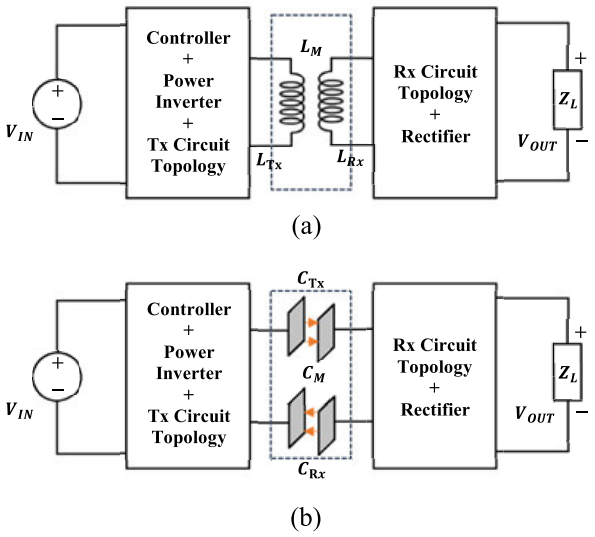

FIGURE 20. Basic setup for a WPT system showing (a) inductive power transfer (IPT) and (b) capacitive power transfer (CPT).

of topology exist. The primary circuit is connected to a primary coupler (Tx) that wirelessly transfers the power to a secondary coupler (Rx). The secondary coupler, in turn, is connected to a secondary circuit whose output is fed into (iv) a rectifier that delivers a DC voltage V_{OUT} to the load. Like the primary side, multiple choices of topology also exist for the secondary circuit.

Many kinds of inverter architectures exist [71], [72], [73], but most WPT applications typically use half-bridge or full-bridge inverters configured using two or four MOSFETs, respectively. The MOSFETs contain either gallium arsenide or gallium nitride, the later having better efficiency and higher power density due to its low electron mobility [116]. In typical WPT applications, the operating frequency of the waveform can range from the low kHz to the low MHz. Compensation components must be chosen: (i) to ensure that the input has a lower VA rating for maximum PTE to the load, (ii) to tolerate Tx-to-Rx misalignment, and (iii) to avoid frequency splitting [79], [120]. Some of the passive components have to be inductive and others capacitive, with the circuit topology such that they resonate together at the same operating frequency generated by the inverter.

In addition, the primary and the secondary couplers contain a non-metallic interface. The interface is either capacitive or inductive depending on whether the modality is IPT or CPT. The contact interface has a mutual inductance L_M for IPT and mutual capacitance C_M for CPT.

For both setups shown in Fig. 20, designing the WPT system for the maximum PTE is the main goal. Therefore, not only is it important to minimize the component count, but also that the chosen components be small in size. The designs of inverters, timing sequences, and rectifiers as well as the choices of the topologies of the primary and secondary circuits for both IPT and CPT have been covered extensively in literature [79], [80], [81], [82], [83], [84].

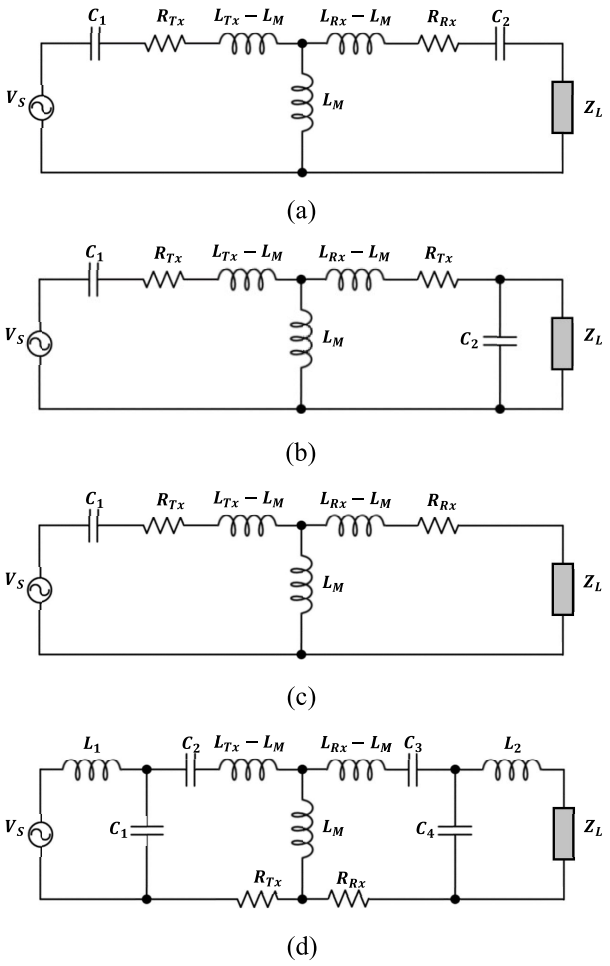

FIGURE 21. Four circuit topologies for NMCs: (a) SS-topology, (b) SP-topology, (c) SN-topology, and (d) LCC-LCC-topology. Circuit topologies for NMCs do not need to be designed to address common WPT issues such as misalignment, power transfer over large distances, or multi-coil systems.

For NMCs, the three main design challenges for power transfer are:

(1) very poor PTE over a fixed Tx and Rx separation,
(2) power-handling limitations on Tx and Rx, and
(3) thermal dissipation.

The first design challenge for NMCs is due to the small form factor whereby both D_{out}^{Tx} and D_{out}^{Tx} are physically restricted. Since the self-inductance of an inductor coil depends on the physical size, this results in restrictions on the self-inductances L_{Tx} and L_{Rx} of the two coils. The mutual inductance L_M between the Tx and Rx coils in Fig. 20(a) is defined as

$$L_M = k\,(L_{\mathrm{Tx}}L_{\mathrm{Rx}})^{-1/2}\,, \tag{15}$$

where k is the coupling coefficient [118]. As the PTE is strongly dependent on L_M, restrictions on D_{out}^{Tx} and D_{out}^{Tx} are restrictions on PTE.

The mutual capacitance C_M between the transmitter capacitor C_{Tx} and the receiver capacitor C_{Rx} in Fig. 20(b) is defined by

$$C_M = [(P_{11}+P_{22}) - (P_{12}+P_{21})]^{-1}\,, \tag{16}$$

where P_{11}, P_{12}, P_{21}, and P_{22} are the coefficients of potential from the elastance matrix for capacitors C_{Tx} and C_{Rx} [121]. Like L_M in IPT, C_M strongly affects PTE in CPT systems.

The second design challenge for NMCs is also related to small form factor. If the power requirements of the system are greater than what a small coupler can handle, the NMC may not be technically feasible for certain applications. CPT allows larger power-handling capacity than IPT does relative to the coupler's physical size. However, small plates in the capacitors C_{Tx} and C_{Rx} will deliver a mutual capacitance C_M that is too small. IPT requires materials besides copper that can withstand higher power densities, which may be uneconomical.

The third design challenge for NMCs is related to the second. High temperatures arise when the power density is large. Therefore, thermal dissipation characteristics must be included in the design of IPT systems.

The remainder of this section focuses on IPT systems and the ways to surmount the three major design challenges. Analogous issues arise for CPT systems, as the reader will easily surmise.

B. WPT CIRCUIT TOPOLOGIES FOR NMCS

The choice of circuit topology is critical for tuning a WPT circuit. This choice depends on the category (SISO, MISO, SIMO, or MIMO), the desired output for constant voltage or constant current, changes in load, tolerance to Tx and Rx misalignment, etc. Many methods have been devised to address each of these factors [84], but many do not apply to NMCs. In fact, the choices of circuit topology for NMCs can be narrowed down to only a few.

Since form factors play an important role in NMCs, circuit topologies that minimize component count are ideal. Misalignment is irrelevant to NMCs; as is evident from the USB flash-drive example in Fig. 12, the plug and receptable will be coaxial in the same location each time they are mated and will also be very close to each other. Therefore, circuit topologies designed with high misalignment tolerance, which typically have a higher component count, or circuit topologies designed for a large separation distance between Tx and Rx can also be eliminated as choices for NMCs.

For NMCs, the circuit topologies must have a high tolerance to changes in load. There will be applications that may require a constant voltage or constant current (or both) where the maximum PTE can be realized with high stability and immunity to frequency splitting. Therefore, the four circuit topologies with the lowest component count to meet this criterion for NMCs are: series-series (SS), series-parallel (SP), series-none (SN), and LCC-LCC. Figure 21 shows these four circuit topologies.

For each circuit topology in Fig. 21, V_S is the AC source voltage generated by the inverter, $L_{Tx}-L_M$ and $L_{Rx}-L_M$ are the linkage inductances on the primary and secondary sides, respectively, and Z_L is the load impedance. Each inductor will have a parasitic resistance denoted by R_{Tx} and R_{Rx}. All capacitors in Fig. 21 compensate for the accompanying inductors and give rise to resonances.

The angular resonance frequency $\omega_0 = 1/\sqrt{L_{Tx}C_1} = 1/\sqrt{L_{Rx}C_2}$ of the SS-topology in Fig. 21(a) is weakly affected by changes in Z_L. For this reason alone, the SS-topology is ideal for use in NMC applications, compared to other topologies with only two compensation circuit elements. Maximum PTE can be realized at both low and high frequencies for smaller magnitudes of Z_L. Another advantage of SS-topology over other circuit topologies is its superior stability when both couplers are equal in size (i.e., $D_{out}^{Tx} = D_{out}^{Rx}$). For NMCs this means more flexibility in design and the two inductors can be chosen to be identical. This added flexibility does not exist for other circuit topologies. Since C_2 is in series on the receiving side, the SS-topology functions as a constant-current source for Z_L.

Higher stability at higher magnitudes of Z_L is possible for the SP-topology in Fig. 21(b) in comparison to the SS-topology. Moreover, because C_2 is in parallel with Z_L, the SP-topology functions as a constant-voltage source for Z_L. If the NMC design requires $D_{out}^{Tx} > D_{out}^{Rx}$, SP-topology delivers higher performance relative to the SS-topology [122].

The SN-topology shown in Fig. 21(c) is commonly referred to as *primary side series*, because it only has a series compensation capacitor on the primary side and no compensation on the secondary side. For this reason, the SN-topology has the lowest possible component count of all circuit topologies and is often used for biomedical applications [79]. The same reason also makes SN-topology ideal for NMC applications. The physical conditions where this topology is ideal is when the gap g between the two inductors is very small and the coupling coefficient k is large. In addition, the quality factors (Q-factors) of both inductors are very high. When these conditions hold, the SN-topology delivers performance characteristics similar to the SS-topology [123]. However, if the operating angular

frequency becomes high enough such that the L_{Rx} resonates with its internal parasitic capacitance, the SN-topology delivers the same performance as the SP-topology [124].

Figure 21(d) shows the LCC-LCC topology. The higher component count may render it inappropriate for certain NMC applications. However, the LCC-LCC topology has superior stability in PTE over changes in ω_0 and Z_L. Also, the LCC-LCC topology is flexible when choosing the compensation elements. In the case where $L_{Tx} = L_{Rx}$, and the compensation inductors can be chosen such that $L_1 = L_2 = L_{Rx}$, all four compensation capacitors in Fig. 22(d) will be equal according to $C_1 = C_2 = C_3 = C_4 = 1/\omega_0^2 L_2$.

C. CHARACTERIZATION PROCEDURE FOR NMCs

Circuit topologies are critical to the design of any WPT system, but they do nothing to help surmount the three design challenges for NMCs stated in Section V-A. To surmount these challenges, (i) ways to improve PTE when g is fixed without increasing the component count are needed and (ii) the electrical power density and the thermal power density of both inductors need to be increased without increasing their physical size. The best way to achieve these goals is to increase the Q-factor of both inductors using materials other than copper. The Q-factors

$$Q_{Tx} = \frac{\omega_0 L_{Tx}}{R_{Tx}}, \tag{17a}$$

and

$$Q_{Rx} = \frac{\omega_0 L_{Rx}}{R_{Rx}} \tag{17b}$$

hold for the Tx coil and Rx coils, respectively.

Many NMC applications will have a fixed value of ω_0 due to industry regulations. Therefore, a high Q-factor requires higher inductance, lower (parasitic) resistance, or both. Knowing how much the Q-factor needs to be increased (if at all) is important for the cost estimates in the NMC design process. Therefore, it is important to fully characterize the electrical performance for any NMC design conforming to the physical space constraints.

For that purpose, the relationship between PTE and g must be understood. This is a three-step process that involves: first, the establishment of a relationship between find PTE and L_M for the chosen circuit topology; second, the establishment of a relationship between L_M and g for the chosen inductor geometry; and third, the combination of the two in order to relate PTE and g.

As an example, consider the evaluation of SS-topology in Fig. 21(a) using Kirchhoff's laws. The input power $P_{IN} = |I_S|^2 \, Re\{Z_{IN}\}/2$ and the output power $P_{OUT} = |I_L|^2 \, Re\{Z_L\}/2$, where I_S is the source current, I_L is the load current, and Z_{IN} is the input impedance as seen by the source. Assuming that $C_1 = C_2 = C$ and $L_{Tx} = L_{Rx} = L$ for the SS-topology, we get

$$PTE_{SS} = \frac{R_L}{(R_{Rx} + R_L)\left[\frac{(R_{Rx}+R_L)R_{Tx}}{\omega_0^2 L_M^2} + 1\right]}, \tag{18}$$

for power transfer at the operating angular frequency, with $\omega_o^2 LC = 1$ and $R_L = Re\{Z_L\}$. When both the Tx and Rx coils are identical, $Q_{Tx} = Q_{Rx} = Q$, $R_{Tx} = R_{Rx} = R = \omega_0 L Q^{-1}$, and (18) becomes

$$PTE_{SS} = \frac{R_L}{(\omega_0 L Q^{-1} + R_L)\left[\frac{(\omega_0 L Q^{-1}+R_L)L}{\omega_0 L_M^2 Q} + 1\right]}. \tag{19}$$

With $C = 1\text{nF}$, $R = 0.6\Omega$, $R_L = 50\Omega$, $f_0 = \omega_0/2\pi = 1.2\text{MHz}$, Fig. 22(a) shows that PTE_{SS} first rises steeply and then saturates as L_M increases from 0 to 18 μH. Typically, the knee in such plots occurs when $k \cong 0.3$ [125].

The inter-coil axial distance g is fixed when the plug and the receptacle are mated. As a result, the Tx and Rx coils must be carefully chosen. Different inductor coil shapes give rise to different self-inductances and therefore different mutual inductance by (15). Therefore, the determination of the coil shape is a very important step.

The relationship between L_M and g for any two coils is defined by the Neumann formula

$$L_M = \frac{\mu_o}{4\pi} \iint \frac{d\boldsymbol{l}_{Tx} \cdot d\boldsymbol{l}_{Rx}}{r}, \tag{20}$$

where $d\boldsymbol{l}_{Tx}$ and $d\boldsymbol{l}_{Rx}$ are differential wire lengths in the two coils, and r is the distance between the location of $d\boldsymbol{l}_{Tx}$ on the Tx coil and the location of $d\boldsymbol{l}_{Rx}$ on the Rx coil [126]. Application of (19) to the Archimedean spirals used for the power inductors in Fig. 12 for the USB application has been considered in detail in Ref. [127]. With both coils having an inner diameter 4 mm, outer diameter 8.3 mm, and screw pitch 0.15 mm, the variation of L_M with g is given in Fig. 22(b). L_M decreases hyperbolically as g increases.

Combining the information in Figs. 22(a) and (b), we obtain the variation of PTE_{SS} with g depicted in Fig. 22(c). Note that PTE_{SS} is large when g is small, and vice versa. So, higher PTE requires as small a value of g as possible.

D. PROPOSED TECHNIQUES TO ENHANCE THE Q-FACTOR FOR NMCs

Industry specifications may require a certain PTE for an NMC to be technically feasible. It is important to quantify the minimum acceptable PTE so that costs can be minimized. As an example, consider two NMC applications. For both, the Tx and Rx coils have reached the maximum number of turns allowed by the NMC geometry, both D_{out}^{Tx} and D_{out}^{Rx} are similarly maximal, and it is required that $PTE \geq 90\%$ when $g = 5\text{mm}$. Initial design delivers $PTE = 81.3\%$ for the first application with D_{out}^{Tx} and D_{out}^{Rx} specified. These outer diameters have been reduced to one fifth for the second application, leading to $PTE = 30\%$.

Since the initial designs must be improved so that $PTE = 90\%$ at least for both applications, the Q-factors will have to be enhanced by different multiples for the two applications. Then, the first application requires only a 10.7% improvement but the second requires that the PTE be tripled.

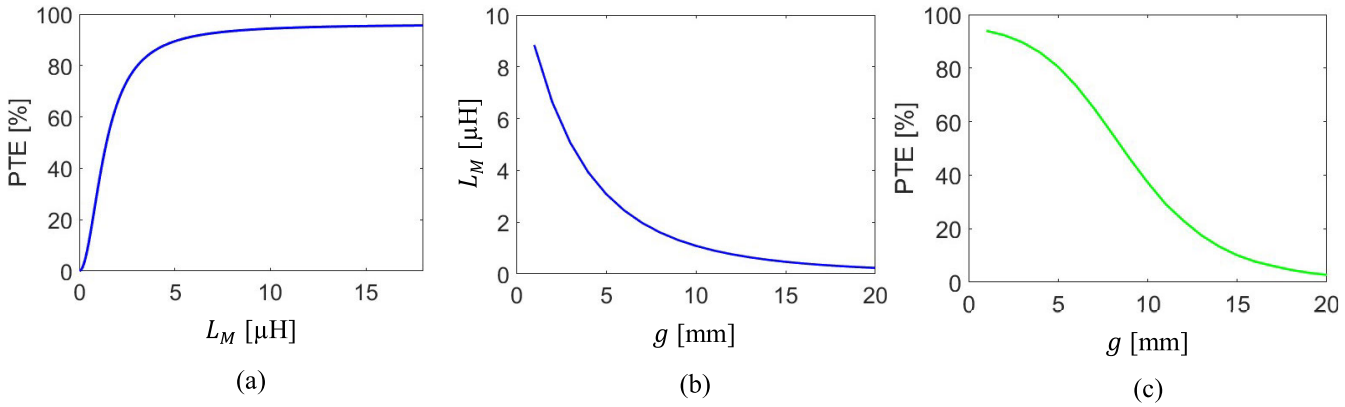

FIGURE 22. Plots of (a) PTE_{SS} vs. L_M from the circuit topology in (18), (b) L_M vs. g from applying the Neumann formula in (20) to the Archimedean spiral geometry, and (c) PTE_{SS} vs. g from numerically combining (a) and (b).

TABLE 2. Proposed methods for enhancing Q-Factor and the associated costs.

Ref.	Image	Method	Q-factor or PTE	Carbon Footprint Cost	Component Count Cost	Monetary Cost	$\mathfrak{D}_r = \frac{D_{out}}{g}$
[128]	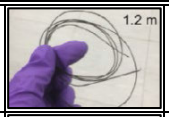	CNT Wire	+39% (Q-factor)	Low	Low	High	$\mathfrak{D}_r > 1$
[129]	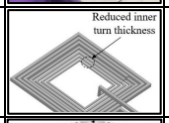	Coil Thickness Variation	+11.5% (Q-factor)	Medium	Low	Low	$\mathfrak{D}_r > 1$
[130]	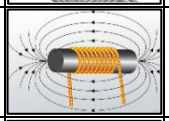	Iron Core	+100x (in PTE)	Medium	Medium	Medium	$\mathfrak{D}_r \leq 1$
[131]	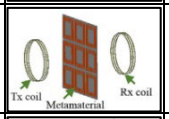	Metamaterial	+400% (in PTE)	Medium	Low	Medium	$\mathfrak{D}_r < 1$
[132]	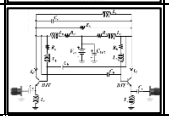	NIC	+7050x (in PTE)	High	High	High	$\mathfrak{D}_r \ll 1$

The cost of improving the Q-factor to meet the 90%-PTE requirement will be much different for the two applications.

Considering the design constraints for NMCs, there are five methods for enhancing the Q-factor: (1) use a coil material with lower parasitic resistance [128], (2) implement a gradient in the wire diameter of each coil [129], (3) increase the permeability of the core and the substrate of each coil [130], (4) employ a metamaterial lens to sculpt the spatial profile of the magnetic field [131], and (5) use a negative impedance converter (NIC) [132]. Each of these five methods delivers a different enhancement level of the Q-factor, and the cost of implementing each method is different.

Table 2 summarizes the performance benefits of different Q-factor-enhancement methods along with the associated costs. Each method has carbon-footprint, component-count, and monetary costs. To properly analyze the costs, a relative distance between the two coils must be considered [83]. With $D_{out}^{Tx} = D_{out}^{Rx} = D_{out}$, this relative distance is given by

$$\mathcal{D}_r = \frac{D_{out}}{g}. \tag{21}$$

The first NMC application needs marginal performance enhancement. Provided that $\mathcal{D}_r > 1$, the first two methods listed in Table 2 can be used. However, if a carbon-nanotube (CNT) wire is used instead of a metallic wire, the present-day cost of adopting the first method are much higher than of the second method.

The second NMC application needs a lot of performance enhancement for it to meet requirements, since $\mathcal{D}_r < 1$. In this case, the last three methods in Table 2 are viable. Note

that using an NIC would have the highest cost of all methods listed in Table 2 and therefore should only be considered as a last option. Very likely, the incorporation of a metamaterial lens is the best option. With these proposed techniques and analysis, the first major design challenge in Sec. V-A for NMCs can be surmounted.

If the first NMC application requires a high-power level such that the small-space restrictions would render small copper coils technically infeasible for both inductors, the first method in Table 2 would be more attractive than the second method. The reason has to do with the superior electrical and thermal properties of CNTs compared to copper. Experiments on WPT systems have shown copper wire to deliver a PTE of 76.5% for 3-A current at 59.2 °C, whereas the CNT wire can deliver a PTE of 83.5% at only 36.8 °C under the same operating conditions [128]. Currently, CNT wire is not a viable candidate for general WPT applications due to the high procurement costs. Other materials such as graphene and borophene are also candidates to enhance the electrical and thermal properties compared to copper in μWPT systems. These new materials are expected to help surmount the second and third major design challenges stated in Sec. V-A for NMCs. Such materials are much cleaner technologies, offer higher sustainability, and can be 3D printed.

VI. CONCLUDING REMARK

Electrical connectors have been commonplace for more than 130 years for the purpose of connecting two electrical devices together with a separable interface, which may make some electrical engineers wonder as to the need for novel connectors. This paper identifies several well-known failure modes associated with electrical contacts, their mitigation requiring tremendous ongoing efforts, especially to accommodate emerging technologies.

Perhaps the best way to eliminate the problems associated with electrical contacts is to eliminate electrical contacts altogether. The NMC concept aims exactly in that direction, using WPT methods. A brief historical overview of the evolution of wireless power transfer was provided in Sec. III, wherein the three technical areas were identified to scale WPT architectures for NMCs. In Secs. IV and V, the NMC concept was categorized into two types: high-speed signal transfer and power transfer. Section IV went into detail on the different ways high-speed NMCs could be realized showing original efforts of using capacitive and inductive coupling modalities and the superior performance of EHF relative to other communication protocols. Based on the physical design limitations of connector applications, NMCs were shown to fall into both near-zone and far-zone technologies in the WPT hierarchy. The concept of μWPT for NMC applications was introduced to modify the currently accepted WPT hierarchy so that the unique requirements of NMCs can be accommodated therein.

Section V outlined the current state of NMC development for power transfer and provided a comparison of four different circuit topologies. With future operational requirements in mind, three major design challenges to the technical feasibility of NMCs were identified. A design process for characterizing NMCs was introduced followed by five methods on how to surmount the three major design challenges. A procedure to characterize NMCs for power transfer was provided, keeping three diverse costs in the foreground. The future of the NMC concept hinges on the development of new materials besides copper for inductor coils. These new materials need to allow higher power density and possess far better thermal properties so that μWPT systems can operate at greater power levels and perform well.

ACKNOWLEDGMENT

The authors would like to thank Frank D. Johns, principal designer at Non-Metallic Connectors, Inc., for his contributions in the creation of the 3D models used for some illustrations in this article. They would also like to thank Gary McCormack for providing the experimental data in Table 1.

REFERENCES

[1] R. S. Mroczkowski, *Electrical Connector Handbook: Technology and Applications*, 1st ed., New York, NY, USA: McGraw-Hill, 1997.
[2] T. T. Smith, "Electric circuit connection," U.S. Patent 311 616, Feb. 3, 1885.
[3] T. A. Edison, "Electric-lamp," U.S. Patent 223 898, Jan. 27, 1880.
[4] J. W. Swan, "Electric lamp," England Patent 234 345, Nov. 9, 1880.
[5] T. A. Edison, "System of electric lighting," U.S. Patent 251 551, Dec. 27, 1881.
[6] H. Hubbell, "Electric switch," U.S. Patent 471 612, Mar. 29, 1892.
[7] H. Hubbell, "Socket for incandescent lamps," U.S. Patent 565 541, Aug. 11, 1896.
[8] H. Hubbel, "Separable attachment plug," U.S. Patent 774 250, Nov. 8, 1904.
[9] W. P. Marr, "Electric wire connector," U.S. Patent 1 583 479, May 4, 1926.
[10] J. L. Rodengen, *The Legend of AMP*. Fort Lauderdale, FL, USA: Write Stuff Enterprises, 1997.
[11] E. J. Neifing, "Historical development of electric connectors," *Electr. Eng.*, vol. 63, no. 12, pp. 925–928, Dec. 1944, doi: 10.1109/EE.1944.6440628.
[12] C. Stewart, "Electrical testing of coaxial radio-frequency cable connectors," *Proc. IRE*, vol. 33, no. 9, pp. 609–619, Sep. 1945, doi: 10.1109/jrproc.1945.231197.
[13] O. A. Boyer and E. Korges, "Connector performance by types [includes discussion]," *Trans. Amer. Inst. Electr. Eng. III, Power App. Syst.*, vol. 75, no. 3, pp. 907–913, Jan. 1956, doi: 10.1109/aieepas.1956.4499382.
[14] *Precedence Research*. Accessed: Mar. 20, 2024. [Online]. Available: https://www.precedenceresearch.com/connector-market
[15] J. Diamond, *Collapse: How Societies Choose to Fail or Succeed*. New York, NY, USA: Penguin Books, 2011.
[16] N. Hadziefendic, J. Trifunovic, and M. Kostic, "Effects of a reduced torque on heating of electrical contacts in plugs and receptacles," *IEEE Trans. Compon., Packag., Manuf. Technol.*, vol. 8, no. 11, pp. 1905–1913, Nov. 2018, doi: 10.1109/TCPMT.2018.2827080.
[17] H.-D. Rubin, V. C. Pascucci, J. Toran, R. Druckenmiller, M. Lipschutz, P. Conde, V. Vasudevan, J. Gupta, Y.-H. Oon, and C. Han, "A standardized reliability evaluation framework for connectors–stress levels and test recommendations," in *Proc. IEEE Holm Conf. Electr. Contacts*, Milwaukee, WI, USA, Sep. 2019, pp. 324–334, doi: 10.1109/HOLM.2019.8923931.
[18] R. D. Malucci, "Fretting corrosion degradation, threshold behavior and contact instability [electrical contacts]," in *Proc. 49th IEEE Holm Conf. Electr. Contacts*, Washington, DC, USA, Nov. 2003, pp. 2–15, doi: 10.1109/HOLM.2003.1246472.
[19] S. Kirkbride, B. Chan, C. Dandl, I. Hsu, B. Martinson, and A. Ryan, "Standardized reliability evaluation framework for connectors," in *Proc. SMTA Int.*, Rosemont, IL, USA, Sep. 2016, pp. 518–528.

[20] H. Yang, Y. Liu, W. Huang, H. Wen, and X. Y. Zhang, "Analysis of passive intermodulation distortion caused by asymmetric electrical contact," *IEEE Trans. Instrum. Meas.*, vol. 71, pp. 1–5, 2022, doi: 10.1109/TIM.2022.3140447.

[21] M. Braunović, V. Konchits, and N. Myshkin, *Electrical Contacts: Fundamentals, Applications and Technology*, 1st ed., Boca Raton, FL, USA: CRC Press, 2007, pp. 6–8.

[22] R. Holm, *Electrical Contacts*, 4th ed., Heidelberg, Germany: Springer, 1967, p. 8.

[23] P. G. Slade, *Electrical Contacts: Principles and Applications*. Boca Raton, FL, USA: CRC Press, 1999.

[24] A. Tiwari, F. Xu, A. Lakhtakia, H. Yamaguchi, and S. T. S. Bukkapatnam, "On colors of stainless-steel surfaces polished with magnetic abrasives," *Appl. Opt.*, vol. 60, no. 9, p. 2549, 2021, doi: 10.1364/ao.419424.

[25] J. A. Greenwood and J. B. P. Williamson, "Contact of nominally flat surfaces," *Proc. Roy. Soc. A*, vol. 295, pp. 300–319, Jan. 1966, doi: 10.1098/rspa.1966.0242.

[26] A. C. Fischer-Cripps, "The Hertzian contact surface," *J. Mater. Sci.*, vol. 34, pp. 129–137, Jan. 2022, doi: 10.1023/A:1004490230078.

[27] N. Ahmadi, L. M. Keer, and T. Mura, "Non-hertzian contact stress analysis for an elastic half space—Normal and sliding contact," *Int. J. Solids Struct.*, vol. 19, no. 4, pp. 357–373, 1983, doi: 10.1016/0020-7683(83)90032-x.

[28] V. C. Pascucci, "Principles and trends in the standardization of connector reliability evaluation," in *Proc. 6th Int. Conf. Rel. Elect. Products Elect. Contacts (ICREPEC)*, Suzhou, China, 2017, pp. 1–11.

[29] K. L. Beach and V. C. Pascucci, "Contact stress relaxation and resistance change relationships in accelerated heat age testing," in *Proc. 46th IEEE Holm Conf. Electr. Contacts*, Chicago, IL, USA, Sep. 2000, pp. 1–17, doi: 10.1109/HOLM.2000.889906.

[30] R. Chaudhary, L. Kaushik, M. H. Azarian, and M. Pecht, "Comparison between synthetic oil lubricants for reducing fretting degradation in lightly loaded gold-plated contacts," *IEEE Trans. Compon., Packag., Manuf. Technol.*, vol. 12, no. 4, pp. 616–626, Apr. 2022, doi: 10.1109/TCPMT.2022.3159572.

[31] D. Hyman and M. Mehregany, "Contact physics of gold microcontacts for MEMS switches," *IEEE Trans. Compon. Packag. Technol.*, vol. 22, no. 3, pp. 357–364, Sep. 1999, doi: 10.1109/6144.796533.

[32] B. Mahon and N. Forbes, *Faraday, Maxwell, and the Electromagnetic Field: How Two Men Revolutionized Physics*. Amherst, NY, USA: Prometheus, 2019.

[33] J. H. Poynting, "On the transfer of energy in the electromagnetic field," *Philos. Trans. Roy. Soc.*, vol. 175, Jan. 1884, doi: 10.1098/rstl.1884.0016.

[34] M. Leone and N. Robotti, "Guglielmo Marconi, Augusto Righi and the invention of wireless telegraphy," *Eur. Phys. J. H*, pp. 1–28, Jul. 2021, doi: 10.1140/epjh/s13129-021-00021-w.

[35] N. Shinohara, "Power without wires," *IEEE Microw. Mag.*, vol. 12, no. 7, pp. S64–S73, Dec. 2011, doi: 10.1109/MMM.2011.942732.

[36] C. Susskind, "The early history of electronics IV. First radiotelegraphy experiments," *IEEE Spectr.*, vol. S-6, no. 8, pp. 66–70, Aug. 1969, doi: 10.1109/MSPEC.1969.5213634.

[37] P. K. Bondyopadhyay, "Guglielmo marconi—The father of long distance radio communication—An engineer's tribute," in *Proc. 25th Eur. Microw. Conf.*, Bologna, Italy, Oct. 1995, pp. 879–885, doi: 10.1109/euma.1995.337090.

[38] G. Marconi, "Improvements in transmitting electrical impulses and signals and in apparatus therefor," British Patent 12 039, Mar. 12, 1896.

[39] N. Tesla, *The Transmission of Electric Energy Without Wires* (The Thirteenth Anniversary Number of the Electrical World and Engineer). New York, NY, USA: McGraw-Hill, 1904.

[40] N. Tesla, *Experiments With Alternate Current of High Potential and High Frequency*. New York, NY, USA: McGraw-Hill, 1904.

[41] M. J. Seifer, *Wizard: The Life and Times of Nikola Tesla: Biography of a Genius*. New York, NY, USA: Citadel Publishers, 2016.

[42] W. C. Brown, "Free-space transmission," *IEEE Spectr.*, vol. S-1, no. 10, pp. 86–91, Oct. 1964, doi: 10.1109/MSPEC.1964.6501195.

[43] H. Hertz, *Dictionary of Scientific Biography*, vol. 4. New York, NY, USA: Charles Scribners, 1972, pp. 340–349.

[44] J. Dai and D. C. Ludois, "A survey of wireless power transfer and a critical comparison of inductive and capacitive coupling for small gap applications," *IEEE Trans. Power Electron.*, vol. 30, no. 11, pp. 6017–6029, Nov. 2015, doi: 10.1109/TPEL.2015.2415253.

[45] E. L. Ginzton, "Retrospective: The $100 idea: How Russell and sigurd varian, with the help of William Hansen and a $100 appropriation, invented the klystron," *IEEE Spectr.*, vol. S-12, no. 2, pp. 30–39, Feb. 1975, doi: 10.1109/MSPEC.1975.6368703.

[46] G. Caryotakis, "The klystron: A microwave source of surprising range and endurance," *Phys. Plasmas*, vol. 5, no. 5, pp. 1590–1598, May 1998, doi: 10.1063/1.872826.

[47] H. A. H. Boot and J. T. Randall, "Historical notes on the cavity magnetron," *IEEE Trans. Electron Devices*, vol. ED-23, no. 7, pp. 724–729, Jul. 1976, doi: 10.1109/T-ED.1976.18476.

[48] P. Lu, M. Wagih, G. Goussetis, N. Shinohara, and C. Song, "A comprehensive survey on transmitting antenna systems with synthesized beams for microwave wireless power transmission," *IEEE J. Microw.*, vol. 3, no. 4, pp. 1081–1101, Jun. 2023, doi: 10.1109/JMW.2023.3285825.

[49] E. Moisello, A. Liotta, P. Malcovati, and E. Bonizzoni, "Recent trends and challenges in near-field wireless power transfer systems," *IEEE Open J. Solid-State Circuits Soc.*, vol. 3, pp. 197–213, 2023, doi: 10.1109/OJSSCS.2023.3313575.

[50] J. Garnica, R. A. Chinga, and J. Lin, "Wireless power transmission: From far field to near field," *Proc. IEEE*, vol. 101, no. 6, pp. 1321–1331, Jun. 2013, doi: 10.1109/JPROC.2013.2251411.

[51] W. C. Brown, J. F. Skowron, G. H. Macmaster, and J. W. Buckley, "The super power CW amplitron," in *IEDM Tech. Dig.*, Washington, DC, USA, Mar. 1963, p. 52, doi: 10.1109/iedm.1963.187384.

[52] W. C. Brown, "The history of wireless power transmission," *Sol. Energy*, vol. 56, no. 1, pp. 3–21, Jan. 1996, doi: 10.1016/0038-092x(95)00080-b.

[53] W. C. Brown, "The history of power transmission by radio waves," *IEEE Trans. Microw. Theory Techn.*, vol. MTT-32, no. 9, pp. 1230–1242, Sep. 1984, doi: 10.1109/TMTT.1984.1132833.

[54] D. Christiansen, "Spectral lines: The space shuffle," *IEEE Spectr.*, vol. S-19, no. 9, p. 29, Sep. 1982, doi: 10.1109/MSPEC.1982.6366996.

[55] W. C. Brown, "Free-space microwave power transmission study, combined phase III and final report," NASA, Washington, DC, USA, Raytheon Tech. Rep. PT-4601, 1975.

[56] J. G. Bolger, F. A. Kirsten, and L. S. Ng, "Inductive power coupling for an electric highway system," in *Proc. 28th IEEE Veh. Technol. Conf.*, Denver, CO, USA, Mar. 1978, pp. 137–144, doi: 10.1109/VTC.1978.1622522.

[57] J. G. Bolger, L. S. Ng, D. B. Turner, and R. I. Wallace, "Testing a prototype inductive power coupling for an electric highway system," in *Proc. 29th IEEE Veh. Technol. Conf.*, Arlington Heights, IL, USA, Mar. 1979, pp. 48–56, doi: 10.1109/VTC.1979.1622664.

[58] H. R. Ross, "Roadway-powered electric vehicle system," U.S. Patent 5 669 470, Sep. 23, 1997.

[59] H. Abe, H. Sakamoto, and K. Harada, "A noncontact charger using a resonant converter with parallel capacitor of the secondary coil," in *Proc. 13th Annu. Appl. Power Electron. Conf. Expo.*, vol. 1, Anaheim, CA, USA, 1998, pp. 136–141, doi: 10.1109/apec.1998.647681.

[60] H. Sakamoto and K. Harada, "A novel circuit for non-contact charging through electro-magnetic coupling," in *Proc. 23rd Annu. IEEE Power Electron. Spec. Conf.*, vol. 1, Toledo, Spain, Jul. 1992, pp. 168–174, doi: 10.1109/PESC.1992.254708.

[61] H. Sakamoto and K. Harada, "A novel converter for non-contact charging with electromagnetic coupling," *IEEE Trans. Magn.*, vol. 29, no. 6, pp. 3228–3230, Nov. 1993, doi: 10.1109/20.281145.

[62] A. Kawamura, K. Ishioka, and J. Hirai, "Wireless transmission of power and information through one high-frequency resonant AC link inverter for robot manipulator applications," *IEEE Trans. Ind. Appl.*, vol. 32, no. 3, pp. 503–508, Jun. 1996, doi: 10.1109/28.502160.

[63] Y. Hiraga, J. Hirai, Y. Kaku, Y. Nitta, A. Kawamura, and K. Ishioka, "Decentralized control of machines with the use of inductive transmission of power and signal," in *Proc. IEEE Ind. Appl. Soc. Annu. Meeting*, vol. 2, Denver, CO, USA, Oct. 1994, pp. 875–881, doi: 10.1109/IAS.1994.377521.

[64] J. Hirai, Y. Hiraga, K. Hirose, Y. Nitta, H. Hamamoto, and K. Nomura, "Noncontacting electric power transfer apparatus, noncontacting signal transfer apparatus, split-type mechanical apparatus employing these transfer apparatus and a control method for controlling same," U.S. Patent 5 770 936, Jun. 23, 1998.

[65] K. W. Klontz, D. M. Divan, D. W. Novotny, and R. D. Lorenz, "Contactless power delivery system for mining applications," in *Proc. Conf. Rec. IEEE Ind. Appl. Soc. Annu. Meeting*, vol. 2, Dearborn, MI, USA, Oct. 1991, pp. 1263–1269, doi: 10.1109/IAS.1991.178024.

[66] J. Gozalvez, "WiTricity—The wireless power transfer [mobile radio]," *IEEE Veh. Technol. Mag.*, vol. 2, no. 2, pp. 38–44, Jun. 2007, doi: 10.1109/MVT.2007.913285.

[67] S. Scorcioni, L. Larcher, and A. Bertacchini, "A reconfigurable differential CMOS RF energy scavenger with 60% peak efficiency and −21 dBm sensitivity," *IEEE Microw. Wireless Compon. Lett.*, vol. 23, no. 3, pp. 155–157, Mar. 2013, doi: 10.1109/LMWC.2013.2243376.

[68] T. Umeda, H. Yoshida, S. Sekine, Y. Fujita, T. Suzuki, and S. Otaka, "A 950-MHz rectifier circuit for sensor network tags with 10-m distance," *IEEE J. Solid-State Circuits*, vol. 41, no. 1, pp. 35–41, Jan. 2006, doi: 10.1109/JSSC.2005.858620.

[69] H. Nakamoto, D. Yamazaki, T. Yamamoto, H. Kurata, S. Yamada, K. Mukaida, T. Ninomiya, T. Ohkawa, S. Masui, and K. Gotoh, "A passive UHF RF identification CMOS tag IC using ferroelectric RAM in 0.35-μm technology," *IEEE J. Solid-State Circuits*, vol. 42, no. 1, pp. 101–110, Jan. 2007, doi: 10.1109/JSSC.2006.886523.

[70] G. Papotto, F. Carrara, and G. Palmisano, "A 90-nm CMOS threshold-compensated RF energy harvester," *IEEE J. Solid-State Circuits*, vol. 46, no. 9, pp. 1985–1997, Sep. 2011.

[71] A. K. Moghaddam, J. H. Chuah, H. Ramiah, J. Ahmadian, P.-I. Mak, and R. P. Martins, "A 73.9%-efficiency CMOS rectifier using a lower DC feeding (LDCF) self-body-biasing technique for far-field RF energy-harvesting systems," *IEEE Trans. Circuits Syst. I, Reg. Papers*, vol. 64, no. 4, pp. 992–1002, Apr. 2017, doi: 10.1109/TCSI.2016.2623821.

[72] Y.-H. Lam, W.-H. Ki, and C.-Y. Tsui, "Integrated low-loss CMOS active rectifier for wirelessly powered devices," *IEEE Trans. Circuits Syst. II, Exp. Briefs*, vol. 53, no. 12, pp. 1378–1382, Dec. 2006, doi: 10.1109/TCSII.2006.885400.

[73] U. Karthaus and M. Fischer, "Fully integrated passive uhf RFID transponder ic with 16.7-μ minimum RF input power," *IEEE J. Solid-State Circuits*, vol. 38, no. 10, pp. 1602–1608, Oct. 2003, doi: 10.1109/JSSC.2003.817249.

[74] J. Yi, W.-H. Ki, and C.-Y. Tsui, "Analysis and design strategy of UHF micro-power CMOS rectifiers for micro-sensor and RFID applications," *IEEE Trans. Circuits Syst. I, Reg. Papers*, vol. 54, no. 1, pp. 153–166, Jan. 2007, doi: 10.1109/TCSI.2006.887974.

[75] T. Le, K. Mayaram, and T. Fiez, "Efficient far-field radio frequency energy harvesting for passively powered sensor networks," *IEEE J. Solid-State Circuits*, vol. 43, no. 5, pp. 1287–1302, May 2008, doi: 10.1109/JSSC.2008.920318.

[76] D. Cavalheiro, F. Moll, and S. Valtchev, "Insights into tunnel FET-based charge pumps and rectifiers for energy harvesting applications," *IEEE Trans. Very Large Scale Integr. (VLSI) Syst.*, vol. 25, no. 3, pp. 988–997, Mar. 2017, doi: 10.1109/TVLSI.2016.2617203.

[77] A. Mohan, S. Mondal, S. S. Dan, and R. P. Paily, "Design considerations for efficient realization of rectifiers in microscale wireless power transfer systems: A review," *IEEE Sensors J.*, vol. 23, no. 18, pp. 20691–20704, Sep. 2023, doi: 10.1109/JSEN.2022.3222938.

[78] N. Ashraf, S. A. Sheikh, S. A. Khan, I. Shayea, and M. Jalal, "Simultaneous wireless information and power transfer with cooperative relaying for next-generation wireless networks: A review," *IEEE Access*, vol. 9, pp. 71482–71504, 2021, doi: 10.1109/ACCESS.2021.3078703.

[79] A. Sagar, A. Kashyap, M. A. Nasab, S. Padmanaban, M. Bertoluzzo, A. Kumar, and F. Blaabjerg, "A comprehensive review of the recent development of wireless power transfer technologies for electric vehicle charging systems," *IEEE Access*, vol. 11, pp. 83703–83751, 2023, doi: 10.1109/ACCESS.2023.3300475.

[80] W. Adepoju, I. Bhattacharya, M. Sanyaolu, M. E. Bima, T. Banik, E. N. Esfahani, and O. Abiodun, "Critical review of recent advancement in metamaterial design for wireless power transfer," *IEEE Access*, vol. 10, pp. 42699–42726, 2022, doi: 10.1109/ACCESS.2022.3167443.

[81] B. Clerckx, R. Zhang, R. Schober, D. W. K. Ng, D. I. Kim, and H. V. Poor, "Fundamentals of wireless information and power transfer: From RF energy harvester models to signal and system designs," *IEEE J. Sel. Areas Commun.*, vol. 37, no. 1, pp. 4–33, Jan. 2019, doi: 10.1109/JSAC.2018.2872615.

[82] K. Jin and W. Zhou, "Wireless laser power transmission: A review of recent progress," *IEEE Trans. Power Electron.*, vol. 34, no. 4, pp. 3842–3859, Apr. 2019, doi: 10.1109/TPEL.2018.2853156.

[83] M. Rehman, S. Mirsaeidi, N. M. Nor, M. A. Koondhar, M. A. A. M. Zainuri, Z. M. Alaas, E. Tag-Eldin, N. A. Ghamry, and M. M. R. Ahmed, "A review of inductive power transfer: Emphasis on performance parameters, compensation topologies and coil design aspects," *IEEE Access*, vol. 11, pp. 144978–145010, 2023, doi: 10.1109/ACCESS.2023.3344041.

[84] X. Lu, P. Wang, D. Niyato, D. I. Kim, and Z. Han, "Wireless charging technologies: Fundamentals, standards, and network applications," *IEEE Commun. Surveys Tuts.*, vol. 18, no. 2, pp. 1413–1452, 2nd Quart., 2016, doi: 10.1109/COMST.2015.2499783.

[85] *IEEE Standard for Safety Levels With Respect to Human Exposure to Radio Frequency Electromagnetic Fields, 3 KHz to 300 GHz*, IEEE Standard C95.1-1991, 1992.

[86] C. A. Balanis, *Antenna Theory: Analysis and Design*, 4th ed., Hoboken, NJ, USA: Wiley, 2016, pp. 31–33.

[87] Y. Rahmat-Samii, L. I. Williams, and R. G. Yaccarino, "The UCLA bi-polar planar-near-field antenna-measurement and diagnostics range," *IEEE Antennas Propag. Mag.*, vol. 37, no. 6, pp. 16–35, Dec. 1995, doi: 10.1109/74.482029.

[88] *System Reference Document (SRdoc); Wireless Power Transmission (WPT) Systems Operating Below 30 MHz*, ETSI Standard TR 103 493-V1.1.1, 2019.

[89] K. Wang and S. Sanders, "Contactless USB—A capacitive power and bidirectional data transfer system," in *Proc. IEEE Appl. Power Electron. Conf. Expo.*, Fort Worth, TX, USA, Mar. 2014, pp. 1342–1347, doi: 10.1109/APEC.2014.6803481.

[90] A. Karalis, J. D. Joannopoulos, and M. Soljačić, "Efficient wireless non-radiative mid-range energy transfer," *Ann. Phys.*, vol. 323, no. 1, pp. 34–48, Jan. 2008, doi: 10.1016/j.aop.2007.04.017.

[91] X. Zhang, H. Meng, B. Wei, S. Wang, and Q. Yang, "An improved three-coil wireless power link to increase spacing distance and power for magnetic resonant coupling system," *EURASIP J. Wireless Commun. Netw.*, no. 131, pp. 1–8, May 2018, doi: 10.1186/s13638-018-1148-8.

[92] B. Wang, W. Yerazunis, and K. H. Teo, "Wireless power transfer: Metamaterials and array of coupled resonators," *Proc. IEEE*, vol. 101, no. 6, pp. 1359–1368, Jun. 2013, doi: 10.1109/JPROC.2013.2245611.

[93] N. Soltani, H. M. Jafari, K. Abdelhalim, H. Kassiri, X. Liu, and R. Genov, "A 21.3%-efficiency clipped-sinusoid UWB impulse radio transmitter with simultaneous inductive powering and data receiving," *IEEE Trans. Biomed. Circuits Syst.*, vol. 16, no. 6, pp. 1228–1238, Dec. 2022, doi: 10.1109/TBCAS.2022.3225304.

[94] V. Forti, C. P. Baldé, R. Kuehr, and G. Bel, "The global e-waste monitor 2020: Quantities, flows and the circular economy potential," United Nations Univ. (UNU)/United Nations Inst. Training Res. (UNITAR), SCYCLE Programme, Int. Telecommun. Union (ITU), Int. Solid Waste Assoc. (ISWA), Geneva, Switzerland, p. 15, 2020.

[95] E. Bogatin, *Signal and Power Integrity—Simplified*, 2nd ed., Boston, MA, USA: Prentice-Hall, 2010, p. 76.

[96] J. S. Benjestorf, "Non-mating connector," U.S. Patent 9 197 292 B2, Nov. 24, 2015.

[97] J. S. Benjestorf and X. Liu, "Non-mating connector for USB a quality waterproof connection," in *Proc. IEEE Int. Conf. Consum. Electron. (ICCE)*, Las Vegas, NV, USA, Jan. 2013, pp. 560–563, doi: 10.1109/ICCE.2013.6487018.

[98] J. Benjestorf, "A new trend in connectivity: Sharing content over multiple channels," *IEEE Consum. Electron. Mag.*, vol. 3, no. 1, pp. 25–31, Jan. 2014, doi: 10.1109/MCE.2013.2284938.

[99] J. S. Benjestorf, "Non-metallic connector for USB receptacle type—A and flash drive," U.S. Patent App. 63/295 047, Dec. 30, 2021.

[100] N. Zannat and P. D. Franzon, "Asymmetric transformer design with multiband frequency response for simultaneous power and data transfer," *IEEE Trans. Compon., Packag., Manuf. Technol.*, vol. 10, no. 4, pp. 644–653, Apr. 2020, doi: 10.1109/TCPMT.2020.2977045.

[101] G. D. McCormack, "Tightly coupled near-field communication-link connector-replacement chips," U.S. Patent 8 554 136 B2, Oct. 8, 2013.

[102] G. D. McCormack and I. A. Kyles, "Scalable high-bandwidth connectivity," U.S. Patent 9 614 590 B2, Apr. 4, 2017.

[103] I. A. Kyles and G. D. McCormack, "Integrated circuit with electromagnetic communication," U.S. Patent 9 444 146 B2, Sep. 13, 2016.

[104] G. D. McCormack, "Distance measurement using EHF signals," U.S. Patent 8 897 700 B2, Nov. 25, 2014.

[105] C. Som and M. A. de Rooij, *Trilogy of Wireless Power Transfer: Basic Principles, WPT Systems and Applications*, 1st ed., Waldenburg, Germany: Würth Elektronik, 2019, pp. 24–27.

[106] C. A. Balanis, *Antenna Theory: Analysis and Design*, 4th ed., Hoboken, NJ, USA: Wiley, 2016, pp. 88–90.
[107] C. A. Balanis, *Advanced Engineering Electromagnetics*, 2nd ed., Hoboken, NJ, USA: Wiley, 2012, pp. 173–177.
[108] S.-H. Woo, J. Lee, and S.-J. Yook, "Effect of a trap zone in reducing nanoparticle contamination of wafers and photomasks in parallel airflowp," *IEEE Trans. Semicond. Manuf.*, vol. 31, no. 1, pp. 87–96, Feb. 2018, doi: 10.1109/TSM.2017.2759091.
[109] S. Banerjee, A. Chaudhuri, and K. Chakrabarty, "Analysis of the impact of process variations and manufacturing defects on the performance of carbon-nanotube FETs," *IEEE Trans. Very Large Scale Integr. (VLSI) Syst.*, vol. 28, no. 6, pp. 1513–1526, Jun. 2020, doi: 10.1109/TVLSI.2020.2976734.
[110] I. W. Agbor, I. Mahbub, and K. Namuduri, "Impact of high temperature on performance of wearable electro-textile antennas," in *Proc. IEEE Texas Symp. Wireless Microw. Circuits Syst. (WMCS)*, Waco, TX, USA, Mar. 2019, pp. 1–5, doi: 10.1109/WMCAS.2019.8732499.
[111] S. S. Roy, A. Paramane, J. Singh, S. Chatterjee, and A. K. Das, "Accurate sensing of insulator surface contamination using customized convolutional neural network," *IEEE Sensors Lett.*, vol. 7, no. 1, pp. 1–4, Jan. 2023, doi: 10.1109/LSENS.2022.3232506.
[112] A. K. Bhattacharyya, *Electromagnetic Fields in Multilayered Structures: Theory and Applications*, 1st ed., Norwood, MA, USA: Artech House, 1994.
[113] Z. Popovic, "Cut the cord: Low-power far-field wireless powering," *IEEE Microw. Mag.*, vol. 14, no. 2, pp. 55–62, Mar. 2013, doi: 10.1109/MMM.2012.2234638.
[114] L. Yang, Y. Zhang, X. Li, B. Feng, X. Chen, J. Huang, T. Yang, D. Zhu, A. Zhang, and X. Tong, "Comparison survey of effects of hull on AUVs for underwater capacitive wireless power transfer system and underwater inductive wireless power transfer system," *IEEE Access*, vol. 10, pp. 125401–125410, 2022, doi: 10.1109/ACCESS.2022.3225541.
[115] Y. Wu, Q. Chen, X. Ren, and Z. Zhang, "Efficiency optimization based parameter design method for the capacitive power transfer system," *IEEE Trans. Power Electron.*, vol. 36, no. 8, pp. 8774–8785, Aug. 2021, doi: 10.1109/TPEL.2021.3049474.
[116] H. Xing, S. Keller, Y.-F. Wu, L. McCarthy, I. P. Smorchkova, D. Buttari, R. Coffie, D. S. Green, G. Parish, S. Heikman, L. Shen, N. Zhang, J. J. Xu, B. P. Keller, S. P. DenBaars, and U. K. Mishra, "Gallium nitride based transistors," *J. Phys., Condens. Matter*, vol. 13, no. 32, pp. 7139–7157, Aug. 2001, doi: 10.1088/0953-8984/13/32/317.
[117] J. Lu, G. Zhu, D. Lin, Y. Zhang, H. Wang, and C. C. Mi, "Realizing constant current and constant voltage outputs and input zero phase angle of wireless power transfer systems with minimum component counts," *IEEE Trans. Intell. Transp. Syst.*, vol. 22, no. 1, pp. 600–610, Jan. 2021, doi: 10.1109/TITS.2020.2985658.
[118] R. C. Dorf and J. A. Svoboda, *Introduction to Electric Circuits*, 7th ed., Hoboken, NJ, USA: Wiley, 2006, p. 526.
[119] I. Smolić and B. Klajn, "Capacitance matrix revisited," *Prog. Electromagn. Res. B*, vol. 92, pp. 1–18, 2021, doi: 10.2528/pierb21011501.
[120] C. Som and M. A. de Rooij, *Trilogy of Wireless Power Transfer: Basic Principles, WPT Systems, and Applications*, 1st ed., Waldenburg, Germany: Würth Elektronik, 2019, pp. 35–39.
[121] W. R. Smythe, *Static and Dynamic Electricity*, 3rd ed., New York, NY, USA: McGraw-Hill, 1968, pp. 36–38.
[122] R. Bosshard, J. W. Kolar, J. Mühlethaler, I. Stevanovic, B. Wunsch, and F. Canales, "Modeling and η–α-Pareto optimization of inductive power transfer coils for electric vehicles," *IEEE J. Emerg. Sel. Topics Power Electron.*, vol. 3, no. 1, pp. 50–64, Mar. 2015, doi: 10.1109/JESTPE.2014.2311302.
[123] S. Cui, Z. Z. Liu, Y. J. Hou, H. Zeng, Z. K. Yue, and L. H. Liang, "Study on efficiency of different topologies of magnetic coupled resonant wireless charging system," *IOP Conf. Ser., Earth Environ. Sci.*, vol. 93, Nov. 2017, Art. no. 012064, doi: 10.1088/1755-1315/93/1/012064.
[124] A. Vulfovich, D. Baimel, and A. Kuperman, "Modified first harmonic approximation-based modeling of SN-compensated inductive power transfer links operating at load-independent-voltage-output frequency," *Simul. Model. Pract. Theory*, vol. 111, Sep. 2021, Art. no. 102340, doi: 10.1016/j.simpat.2021.102340.
[125] G. A. Covic and J. T. Boys, "Modern trends in inductive power transfer for transportation applications," *IEEE J. Emerg. Sel. Topics Power Electron.*, vol. 1, no. 1, pp. 28–41, Mar. 2013, doi: 10.1109/JESTPE.2013.2264473.
[126] D. J. Griffiths, *Introduction to Electrodynamics*, 4th ed., Cambridge, U.K.: Cambridge Univ. Press, 2017, pp. 322–325.
[127] S. Liu, J. Su, and J. Lai, "Accurate expressions of mutual inductance and their calculation of Archimedean spiral coils," *Energies*, vol. 12, no. 10, p. 2017, May 2019, doi: 10.3390/en12102017.
[128] M. A. Tawfik, M. Ehab, K.-T. Kim, C.-G. Lee, P. Junghwan, A. Ahmed, and J.-H. Park, "On using CNTFs-based wires for high frequency wireless power transfer charging systems," *IEEE Trans. Nanotechnol.*, vol. 20, pp. 784–793, 2021, doi: 10.1109/TNANO.2021.3119695.
[129] J.-I. Moon, C. M. Awuah, P. Danuor, and Y.-B. Jung, "Analysis of coil-thickness-variation technique for Q-factor enhancement of rectangular planar coils," *IEEE Trans. Antennas Propag.*, vol. 71, no. 2, pp. 1875–1882, Feb. 2023, doi: 10.1109/TAP.2023.3234985.
[130] L. Wang, Z. Hu, Y.-F. Liu, Y. Pei, and X. Yang, "Multipermeability inductors for increasing the inductance and improving the efficiency of high-frequency DC/DC converters," *IEEE Trans. Power Electron.*, vol. 28, no. 9, pp. 4402–4413, Sep. 2013, doi: 10.1109/TPEL.2012.2228504.
[131] J. Zhou, P. Zhang, J. Han, L. Li, and Y. Huang, "Metamaterials and metasurfaces for wireless power transfer and energy harvesting," *Proc. IEEE*, vol. 110, no. 1, pp. 31–55, Jan. 2022, doi: 10.1109/JPROC.2021.3127493.
[132] T.-H. Kim, G.-H. Yun, W. Lee, and J.-G. Yook, "Highly efficient WPT system with negative impedance converter for Q-factor improvement," *IEEE Access*, vol. 7, pp. 108750–108760, 2019, doi: 10.1109/ACCESS.2019.2933004.

JOSHUA S. BENJESTORF (Senior Member, IEEE) received the B.S. degree in electrical engineering and applied mathematics from the University of the Pacific, Stockton, CA, USA, and the M.S. degree in electrical engineering from The Pennsylvania State University, University Park, PA, USA, where he is currently pursuing the Ph.D. degree in electrical engineering.

With over 15 years of industry experience, he has previously worked for Intel Corporation, Japanese Solderless Terminal (JST), and TE Connectivity, where he has held engineering roles in manufacturing, research and development, and software development. In 2018, he co-founded Non-Metallic Connectors, Inc., Harrisburg, PA, USA, where he is currently the CEO and oversees all aspects of research and development, business development, and fundraising. He was recognized by the Central PA Business Journal as a Forty Under 40 honoree for his entrepreneurial achievements in the connector industry and the development of the non-metallic connector (NMC) concept. His research interests include mathematical modeling, wireless power transfer, metamaterials, antennas, electromagnetics, contactless connectivity, renewable energy, and sustainable engineering.

Mr. Benjestorf is a member of American Association for the Advancement of Science (AAAS) and the Institute of Engineering Technology (IET). He actively serves as a Reviewer for IEEE TRANSACTIONS IN POWER ELECTRONICS and serves on the IEEE Executive Committee, Region 2, Susquehanna section.

VINCENT (VINCE) C. PASCUCCI received the graduate degree in mechanical engineering from the University of Rochester and the M.B.A. degree from The Pennsylvania State University.

He is a consultant in the areas of failure analysis and reliability engineering with specific expertise in electrical connectors. He is a Retired Engineering Fellow at TE Connectivity following a 39-year career where he had roles in connector reliability testing and managing TE's Harrisburg failure analysis laboratory which he founded in 1997 and was recognized with TE Connectivity's Lifetime Achievement Award for his contributions. He has authored numerous papers on connector reliability and has regularly presented his research at academic conferences. He served as US Technical Advisor to the International Electrotechnical Commission (IEC) committees TC48 and SC48B and governor (chair) of SC48B Working Group five responsible for connector testing standards. His work on connector reliability standards in IEC was recognized with an IEC "1906" award for advances in the area of electrical-connector reliability. He is a Technical Advisor at Non-Metallic Connectors, Inc.

JULIO V. URBINA (Senior Member, IEEE) received the B.S. degree in electronics engineering from Universidad Nacional de Ingenieria, Lima, Peru, in 1990, and the M.S. and Ph.D. degrees in electrical engineering from the University of Illinois at Urbana–Champaign, Urbana, IL, USA, in 1996 and 2002, respectively.

From 1989 to 1993, he was with Jicamarca Radio Observatory, Lurigancho-Chosica, Peru. From 2002 to 2006, he was with the University of Arkansas at Little Rock, Little Rock, AR, USA, and Arecibo Observatory, Puerto Rico. In 2006, he joined The Pennsylvania State University, University Park, PA, USA, where he is currently a Professor of electrical engineering. His recent research interests include digital systems and space instrumentation, cognitive radars, software-defined radio and radars, sensors, acquisition, reconfigurable instrumentation, morphware systems, high-performance computer, meteor science, radio wave propagation, space engineering, remote sensing, and radar studies of the atmosphere.

AKHLESH LAKHTAKIA (Fellow, IEEE) received the B.Tech. and D.Sc. degrees in electronics engineering from Banaras Hindu University, Varanasi, India, in 1979 and 2006, respectively, and the M.S. and Ph.D. degrees in electrical engineering from The University of Utah, Salt Lake City, UT, USA.

In 1983, he joined The Pennsylvania State University, University Park, PA, USA, where he is currently an Evan Pugh University Professor of engineering science and mechanics. He has held visiting appointments at Universidad de Buenos Aires (Physics), the University of Glasgow (Mathematics), Imperial College London (Physics), the University of Otago (Physics), the University of Waikato (Management Communication), the Technical University of Denmark (mechanical engineering), Indian Institute of Technology Kanpur (Physics), Indian Institute of Technology BHU (Electronics Engineering and Materials Science), Indian Institute of Technology Bhilai (Electrical Engineering), and The University of Edinburgh (Mathematics). His current research interests include electromagnetics, nanophotonics, surface multiplasmonics, and complex materials, including sculptured thin films and mimumes, forensic science, thin-film photovoltaic solar cells, bioreplication, and sustainability. He has been elected as a fellow of SPIE, the Optical Society of America, American Association for the Advancement of Science, American Physical Society, Institute of Physics, U.K., the IEEE, Royal Society of Chemistry, the Royal Society of Arts, and Sigma Xi. He received the SPIE Technical Achievement Award, in 2010; the Sigma Xi Walston Chubb Award in Innovation, in 2016; the SPIE Smart Materials Lifetime Achievement Award; the Radio Club of America Lifetime Achievement Award; the IEEE APS Distinguished Achievement Award, in 2022; and the SPIE Gold Medal, in 2024. He was a 2022–2023 Jefferson Science Fellow of U.S. Department of State.